REPORT DOCUMENTATION PAGE

Form Approved OMB NO. 0704-0188

1. REPORT DATE (DD-MM-YYYY)	2. REPORT TYPE	3. DATES COVERED (From - To)
	New Reprint	-

4. TITLE AND SUBTITLE
Molecular-level computational investigation of mechanical transverse behavior of p-phenylene terephthalamide (PPTA) fibers

5a. CONTRACT NUMBER
W911NF-09-1-0513

5b. GRANT NUMBER

5c. PROGRAM ELEMENT NUMBER
622105

6. AUTHORS
Mica Grujicic, Subrahmanian Ramaswami, Jennifer Snipes, Ramin Yavari, Gary Lickfield, Chian-Fong Yen, Bryan Cheeseman

5d. PROJECT NUMBER

5e. TASK NUMBER

5f. WORK UNIT NUMBER

7. PERFORMING ORGANIZATION NAMES AND ADDRESSES
Clemson University
Office of Sponsored Programs
300 Brackett Hall, Box 345702
Clemson, SC 29634 -5702

8. PERFORMING ORGANIZATION REPORT NUMBER

9. SPONSORING/MONITORING AGENCY NAME(S) AND ADDRESS (ES)
U.S. Army Research Office
P.O. Box 12211
Research Triangle Park, NC 27709-2211

10. SPONSOR/MONITOR'S ACRONYM(S)
ARO

11. SPONSOR/MONITOR'S REPORT NUMBER(S)
56526-EG.16

12. DISTRIBUTION AVAILIBILITY STATEMENT
Approved for public release; distribution is unlimited.

13. SUPPLEMENTARY NOTES
The views, opinions and/or findings contained in this report are those of the author(s) and should not contrued as an official Department of the Army position, policy or decision, unless so designated by other documentation.

14. ABSTRACT
Purpose – A series of all-atom molecular-level computational analyses is carried out in order to investigate mechanical transverse (and longitudinal) elastic stiffness and strength of p-phenylene terephthalamide (PPTA) fibrils/fibers and the effect various microstructural/topological defects have on this behavior. The paper aims to discuss these issues.
Design/methodology/approach – To construct various defects within the molecular-level model, the relevant open-literature experimental and computational results were utilized, while the

15. SUBJECT TERMS
Fiber transverse properties, Kevlar, Material modeling, PPTA

16. SECURITY CLASSIFICATION OF:			17. LIMITATION OF ABSTRACT	15. NUMBER OF PAGES	19a. NAME OF RESPONSIBLE PERSON
a. REPORT	b. ABSTRACT	c. THIS PAGE			Mica Grujicic
UU	UU	UU	UU		19b. TELEPHONE NUMBER 864-656-5639

Report Title

Molecular-level computational investigation of mechanical transverse behavior of p-phenylene terephthalamide (PPTA) fibers

ABSTRACT

Purpose – A series of all-atom molecular-level computational analyses is carried out in order to investigate mechanical transverse (and longitudinal) elastic stiffness and strength of p-phenylene terephthalamide (PPTA) fibrils/fibers and the effect various microstructural/topological defects have on this behavior. The paper aims to discuss these issues.

Design/methodology/approach – To construct various defects within the molecular-level model, the relevant open-literature experimental and computational results were utilized, while the concentration of defects was set to the values generally encountered under "prototypical" polymer synthesis and fiber fabrication conditions.

Findings – The results obtained revealed: a stochastic character of the PPTA fibril/fiber strength properties; a high level of sensitivity of the PPTA fibril/fiber mechanical properties to the presence, number density, clustering and potency of defects; and a reasonably good agreement between the predicted and the measured mechanical properties.

Originality/value – When quantifying the effect of crystallographic/morphological defects on the mechanical transverse behavior of PPTA fibrils, the stochastic nature of the size/potency of these defects was taken into account.

REPORT DOCUMENTATION PAGE (SF298)
(Continuation Sheet)

Continuation for Block 13

ARO Report Number 56526.16-EG
Molecular-level computational investigation of m...

Block 13: Supplementary Note

Approved for public release; distribution is unlimited.

The current issue and full text archive of this journal is available at
www.emeraldinsight.com/1573-6105.htm

Received 1 November 2012
Revised 31 December 2012
12 January 2013
Accepted 20 January 2013

Molecular-level computational investigation of mechanical transverse behavior of *p*-phenylene terephthalamide (PPTA) fibers

Mica Grujicic, Subrahmanian Ramaswami, Jennifer Snipes and Ramin Yavari
Department of Mechanical Engineering, Clemson University, Clemson, South Carolina, USA

Gary Lickfield
Department of Materials Science, Clemson University, Clemson, South Carolina, USA

Chian-Fong Yen
Army Research Laboratory, Weapons and Materials Research Department, Aberdeen, Maryland, USA, and

Bryan Cheeseman
Department of Mechanical Engineering, Clemson University, Clemson, South Carolina, USA

Abstract

Purpose – A series of all-atom molecular-level computational analyses is carried out in order to investigate mechanical transverse (and longitudinal) elastic stiffness and strength of *p*-phenylene terephthalamide (PPTA) fibrils/fibers and the effect various microstructural/topological defects have on this behavior. The paper aims to discuss these issues.

Design/methodology/approach – To construct various defects within the molecular-level model, the relevant open-literature experimental and computational results were utilized, while the concentration of defects was set to the values generally encountered under "prototypical" polymer synthesis and fiber fabrication conditions.

Findings – The results obtained revealed: a stochastic character of the PPTA fibril/fiber strength properties; a high level of sensitivity of the PPTA fibril/fiber mechanical properties to the presence, number density, clustering and potency of defects; and a reasonably good agreement between the predicted and the measured mechanical properties.

Originality/value – When quantifying the effect of crystallographic/morphological defects on the mechanical transverse behavior of PPTA fibrils, the stochastic nature of the size/potency of these defects was taken into account.

Keywords Fiber transverse properties, Kevlar, Material modeling, PPTA

Paper type Research paper

Multidiscipline Modeling in Materials and Structures
Vol. 9 No. 4, 2013
pp. 462-498

1573-6105
DOI 10.1108/MMMS-11-2012-0018

1. Introduction

The present work deals with high specific-strength, high specific-stiffness *p*-phenylene terephthalamide (PPTA) polymeric fibers such as Kevlar®, Twaron®, etc. These fibers are commonly used in various ballistic-/blast-protection systems with the main requirement being a high level of penetration resistance against large kinetic energy projectiles (e.g. bullets, detonated mine induced soil ejecta, IED or turbine fragments, etc.). Such protective systems/structures are nowadays being designed and developed through an extensive use of computer-aided engineering (CAE) methods and tools which require the knowledge of high-fidelity material constitutive models capable of describing the behavior of fibers and structures under high-rate loading conditions. As will be revealed below, development of such material models requires the recognition of the hierarchical/multi-scale architecture of the fibers and structures. Thus, the main aspects of the present work include:

- high-performance PPTA fibers;
- multi-length-scale architecture of the fibers and related protective structures; and
- development of material-models for use in CAE analyses.

A brief overview of these aspects of the problem at hand is presented in the remainder of this section. It should be noted that the PPTA fibers under investigation are normally used as either thread constituents in two-dimensional or three-dimensional woven-fabric (flexible) protective structures (e.g. "bulletproof vests") or as reinforcements in high-performance (typically, polymer-matrix, "rigid-armor") composites.

High-performance PPTA fibers

PPTA fibers are made from the family of polymeric materials known as polyamides. Polyamides are typically classified as aromatic polyamides or aramids (e.g. Kevlar®, Twaron®, etc.) and non-aromatic polyamides (e.g. nylon-6,6). A pictorial representation of a single PPTA repeat unit, consisting of two phenylene rings/moieties joined by two amide linkages, is shown in Figure 1(a). Figure 1(b) uses the same type of ball-and-stick representation to schematically display the basic PPTA condensation-polymerization reaction. For improved clarity, the atomic species are labeled in this figure. While, in principle, PPTA can appear both in the ("opposite") trans- (Figure 1(a)) and ("on the same side") cis- (not shown for brevity) stereo-isomeric conformations, the latter conformation is rarely observed. This finding is explained by steric hindrance inhibiting the attainment of the cis-conformation, while the trans-conformation promotes formation of lower-energy stretched-out/extended molecules. The presence of large numbers of nearly-parallel molecules, in turn, enables the fibers to take full advantage of the linear character of the molecular back-bone structure and to crystallize, forming PPTA fibrils.

Due to a large difference in electronegativity between oxygen and hydrogen, amide linkages possess large dipole moments and, hence, are prone to forming hydrogen bonds. When such bonds are formed laterally between parallel PPTA molecules/chains, "sheet-like" structures are created. PPTA fibers are commonly found to have a crystalline structure consisting of stacked sheets. However, while hydrogen bonding plays a key role in the formation of the sheets, its contribution to the inter-sheet bonding is generally considered to be minor. Examination of the crystalline

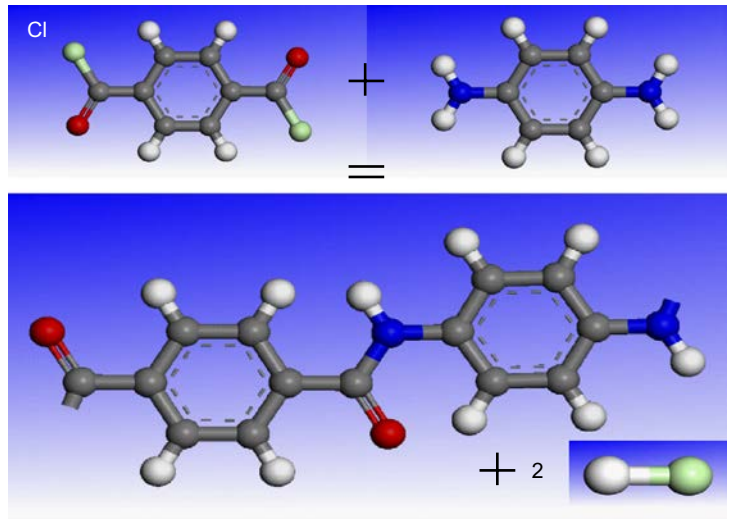

(b)

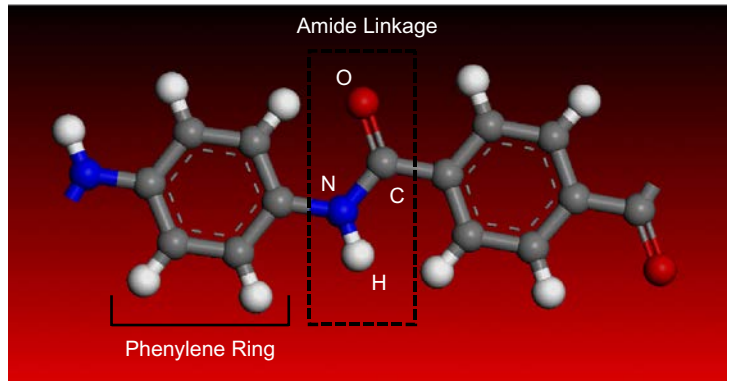

(a)

Figure 1.
(a) Trans- molecular conformations in typical PPTA-based polymeric-material chains/molecules and (b) PPTA condensation polymerization reaction

PPTA fibrils reveals that the sheets are not entirely planar but contain small-amplitude (ca. 40 nm), high wave-length (ca. 250-500 nm) accordion-style "pleats".

Due to their molecular structure, PPTA chains possess high bending stiffness and, hence, do not easily flex. High rigidity of the PPTA molecules is believed to be one of the major factors affecting the microstructure of the PPTA fibers. That is, in contrast to the flexible polymeric molecules which can undergo extensive folding and give rise to the formation of the commonly observed (crystalline + amorphous) two-phase polymeric microstructure, the PPTA fibers typically acquire either a paracrystalline or a fully crystalline microstructure. In the case of the paracrystalline structure, PPTA molecules are all aligned in the same direction but no order exists in a plane orthogonal to this direction. In sharp contrast, in the case of the fully crystalline PPTA fibers, molecules are aligned in all three mutually orthogonal directions. It should also be

noted that the formation of paracrystalline or crystalline structures is promoted by the presence of the planar phenylene and amide groups and by the ability of the adjacent chains to form hydrogen bonds.

Close examination of the PPTA crystal structure reveals that it is of a layered character and consists of parallel (ABABAB. . .) stacked sheets. As mentioned earlier, the sheets are formed due to hydrogen bonding between the adjacent parallel PPTA molecules while the inter-sheet bonding is mainly of the van der Waals (and p-electron weak chemical-bond) type. As clearly established by Wadee *et al.* (2004), Edmunds and Wadee (2005) and Wadee and Edmunds (2005), due to the low strength of the inter-sheet bonding, PPTA crystal structure is prone to the formation of stacking faults and kink bands, and, consequently, PPTA fibers possess inferior longitudinal compressive strength and buckling resistance.

As in most engineering materials, properties of PPTA fibers are greatly affected by the presence of various crystallographic and morphological defects/flaws. The character, size and the number density of these flaws is closely related to the PPTA synthesis and fiber fabrication processes. Details regarding PPTA synthesis and fiber fabrication can be found in the relevant patent literature (Kwolek and du Pont, 1972; Blades, 1973; du Pont, 1983), and a brief overview of these processes was given in our recent work (Grujicic *et al.*, 2011a, b).

The summary of the PPTA synthesis and fiber fabrication processes presented by Grujicic *et al.* (2011a, b) clearly revealed that different types of defects/flaws may be and do get generated within PPTA fibers. Since these defects have a profound effect on the fiber properties, as well as on the properties of coarser-scale fiber-based structures (e.g. yarns, fabrics, plies, laminae and laminates), they were also reviewed by Grujicic *et al.* (2011a, b). A summary of the PPTA fiber most common defects, their dimensionality, their cause, ways of reducing their number density and their typical concentrations is provided in Table I.

Multi-length-scale architecture of PPTA and related protective structures

Detailed examination of PPTA fibers and related protective structures carried out in our recent work (Grujicic *et al.*, 2011b) revealed their high complexity which stems mainly from:

- their hierarchical, multi-length-scale architecture;
- their mechanical response which is often quite non-linear and rate/time-dependent; and
- the operation of complex phenomena/processes (e.g. filament twisting, inter-filament friction and sliding, etc.).

It should be noted that the term "filament" is used here to denote a thread-like entity (typically fibers or yarns) used in the construction of the protective systems. Fibers are typically produced by a polymer-spinning process while a yarn represents a bundle of parallel fibers, often lightly twisted about the yarn axis and held together by wrap-around fibers.

In our recent work (Grujicic *et al.*, 2011a, b), an attempt was made to help clarify the nature of the multi length-scale hierarchy of the PPTA-based protective structures, typically consisting of polymer matrix composite materials reinforced with PPTA filaments. The work identified the existence of (at least) eight length-scales.

Defect class	Defect type	Cause(s)	Defect formation prevention	Number density range
Isolated chain ends (point defect)	—COOH	H_2SO_4 catalyzed hydrolysis causing PPTA chain scission. Na^+ deficiency with respect to complete neutralization of side/end acidic groups	Use concentrated H_2SO_4 for dope preparation. Shorten the fiber wash time	0.35 per PPTA chain for each defect[a] (~350 ppm-mass-based)
	—NH_2	H_2SO_4 catalyzed hydrolysis causing PPTA chain scission. Na^+ deficiency with respect to complete neutralization of side/end acidic groups	Use higher concentration NaOH solution	0.35 per PPTA chain for each defect[a] (~350 ppm-mass-based)
	—COO^-Na^+	COOH neutralization with Na^+	No remedy required since this is one of the preferred chain ends	1.1 per PPTA chain[a] (~1,100 ppm-mass-based)
	—$NH_3^+HSO_4^-$	Sulfonation of the NH_2 chain ends	Increase the H_2SO_4 removal and neutralization rate	0.2 per PPTA chain[a] (~200 ppm-mass-based)
Side groups (point defect)	—SO_3H	Exposure of PPTA in the dope to concentrated H_2SO_4 (sulfonation)	Reduce the H_2SO_4 concentration in the dope	~1,300 ppm (mass-based)
	—$SO_3^-Na^+$	Neutralization of sulfonic acid side groups by NaOH	Remedy may not be required since this side group improves fiber longevity. However, mechanical performance may be compromised	~2,500 ppm (mass-based)
Voids and interstitials (point defects)	Microvoids	Swelling induced by hydration of intra-fibrillar Na_2SO_4	Increase the extent of sodium salt dissolution by prolonged exposure of fibers to boiling water	~150 ppm (mass-based)
	Mobile trapped H_2SO_4	Non-neutralized or unwashed intra-fibrillar H_2SO_4	Thorough washing in hot solvent aqueous bath	~70 ppm (mass-based)
Defect bands (planar defects)	$NH_3^+HSO_4^-$ agglomerated chain ends	Coulombic attraction induced clustering of ion-terminated chain ends	The phenomenon is not well understood so no remedy is obvious	One band every 40-60 nm of fibril (ca. 3,000 ppm-mass-based)

Note: [a]Extruded fibers

Table I.
Classification of the most common defects found in PPTA fibers

A brief description of these length-scales is provided here. In addition, a schematic and supplementary details of the eight microstructural length-scales is shown in Figure 2. For each length-scale, the right column in Figure 2 shows a simple schematic of the material microstructure/architecture along with the labels used to denote the main microstructural constituents. A brief description of the material model(s) used to capture the material behavior at the length-scale in question is provided in the left column. The main features of the eight length scales can be summarized as follows:

(1) At the laminate length-scale, the material is assumed not to possess any discernible microstructural features, i.e. it is completely monolithic/homogenized.

(2) At the stacked-lamina length-scale, the presence of discrete stacked laminae is recognized while the material within each lamina as well as inter-lamina boundaries are kept featureless/homogenized.

(3) At the single-lamina length-scale, recognition is given to the existence of two distinct phases (i.e. the matrix and the reinforcing structure) and their continuity/discreteness while the associated materials are assumed to be featureless/homogenized.

(4) While the constituent materials are still considered as being featureless/homogenized at the fabric unit-cell length-scale, a closer look is given to the architecture of the woven fabric to account for the phenomena such as yarn weaving and crimping, yarn cross-section change, and yarn sliding at the warp-yarn/weft-yarn crossings.

(5) At the yarn length-scale, the internal structure/architecture of each yarn is accounted for explicitly. In other words, yarns are considered as assemblies of nearly parallel fibers/filaments which are mechanically engaged by either the application of a light twist to the yarn or by wrapping a fiber around the fiber/filament assembly. On the other hand, the constituent fibers are treated as featureless/homogenized.

(6) At the fiber length-scale, fibers are considered as assemblies of parallel fibrils (nearly coaxial with the fiber itself) which are held together by non-bond (van der Waals or Coulomb) forces. Fibrils themselves consist of molecular chains tightly bonded into a perfect or nearly perfect crystalline phase.

(7) While at the fibril-level length-scale the material is crystalline or nearly crystalline, it often possesses a variety of microstructural and topological defects and chemical impurities which may significantly alter its properties.

(8) At the molecular-level length-scale, recognition is given to the chemical structure and conformation of the individual molecules interconnected to form longer molecular chains.

Development of material-models for use in CAE analyses

Development of the aforementioned ballistic/blast protection systems is traditionally carried out using legacy knowledge and extensive "fabricate-and-test" procedures. Since this approach is not only associated with higher cost, but often entails significantly longer lead times, it has gradually become complemented by the appropriate cost- and time-efficient CAE analyses. Recent developments in the numerical modeling of

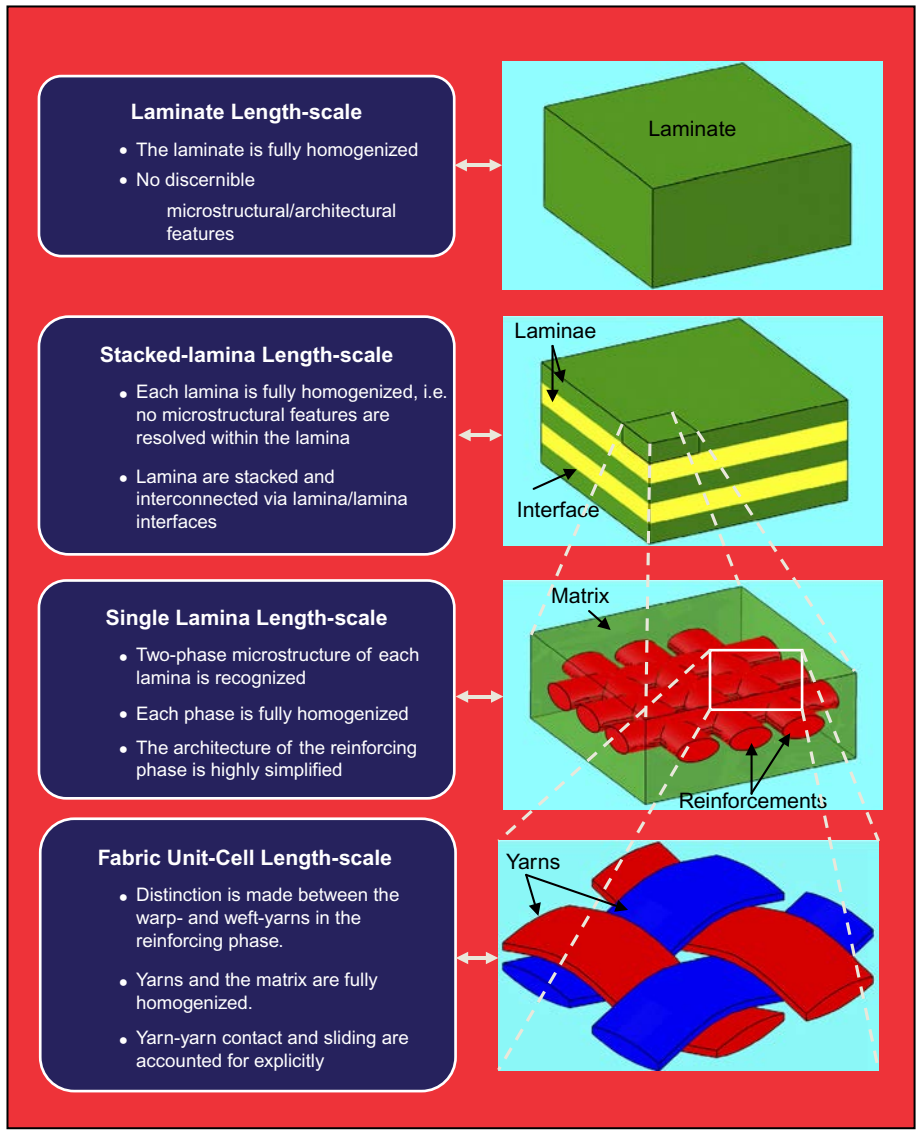

(*continued*)

Figure 2.
Various length-scales and the associated material model assumptions/ simplifications used in the study of polymer-matrix composite materials with high-performance fiber-based structures

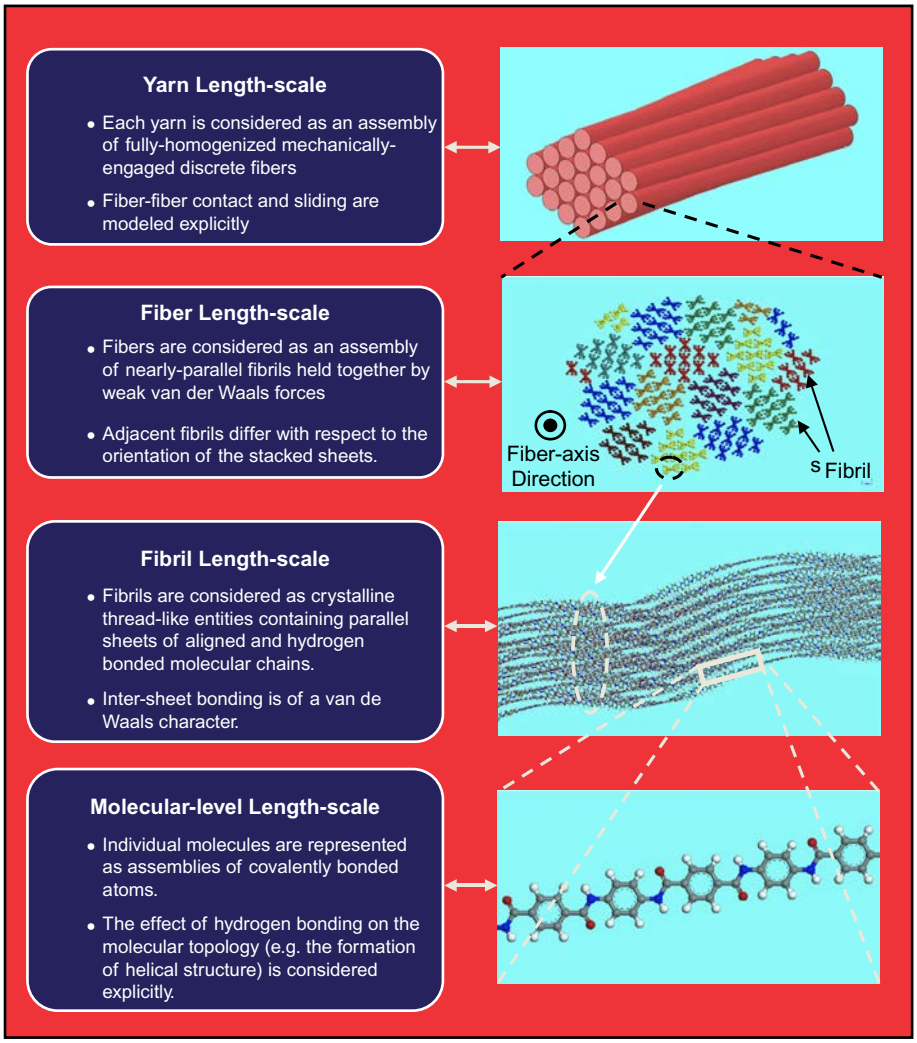

Figure 2.

transient non-linear dynamics phenomena such as those accompanying blast and ballistic loading conditions have further accelerated the use of CAE analyses. However, these analyses themselves suffer from a number of limitations/deficiencies which prevent their wider utilization. Among the key main deficiencies of the current CAE analyses is the inability of the available material models to realistically represent the response of the subject materials under high-deformation-rate, large-strain, high-pressure loading conditions, the type of loading conditions typically encountered during projectile impact events. It is generally believed that shortcomings of the current material models stem from the fact that they do not adequately account for the contribution of various phenomena and processes occurring at different length scales to the overall behavior/performance of the material. In our recent work (Grujicic *et al.*, 2011a, b, 2012, 2013), a preliminary effort was

made to improve PPTA-based material models by accounting for the effect of fiber-scale microstructural features (including the defect structure) on the mechanical performance of the materials at hand. This effort is extended in the present work by addressing more closely the response of PPTA filaments to transverse loading. This type of loading is generally encountered by PPTA filaments residing within the protective systems subjected to ballistic/blast impact.

Examination of the open-domain literature carried out as part of the present work revealed a number of efforts aimed at modeling the blast/ballistic protection offered by PPTA-based systems. Among these efforts, the following appear to be the most note-worthy:

(1) Among the first investigations aimed at predicting the behavior of protective structures (specifically biaxial fabrics) when subjected to ballistic impact loading is the one carried out by Roylance (1973). In this investigation fabric is modeled using pin-jointed orthogonal bars and this oversimplified model was unable to fully account for contributions associated with phenomena such as the weave architecture, surface-finish and inter-yarn friction, etc.

(2) A more comprehensive ballistic fabric model that was proposed by Taylor and Vinson (1990) treats the fabric as a homogeneous, isotropic, and elastic plate, which deforms, under ballistic impact, into the shape of a straight-sided conical shell. The assumption of the material within the plate being homogeneous and isotropic can be considered as a gross (unsupported) oversimplification of the fabric-material microstructure and behavior.

(3) Further improvements in the modeling of ballistic fabric were introduced in the work of Lim *et al.* (2003), who employed a three-element spring-dashpot model to describe a rate-dependent non-linear stress-strain behavior of Twaron®-based fabric and included a strain-rate dependent strain-based failure criterion (Shim *et al.*, 2001).

(4) To account for the fabric architecture and for transverse interaction of crossed yarns, Cunniff and Ting (1999) included in their ballistic fabric model the following specifics:

- warp and weft/fill yarns are modeled independently using elastic rod elements;
- contact elements are used to account for the transverse interaction between the crossing yarns; and
- while in the longitudinal direction the yarns are assumed to behave as linear elastic materials, their transverse behavior is treated as being non-linear/inelastic.

(5) Johnson *et al.* (1999, 2002) attempted to rationalize the transverse behavior of the yarns and found that this behavior is a result of a complex interaction between the inter-fiber contact phenomena and the transverse mechanical response of the fibers themselves.

(6) To help reveal the contribution of the fiber transverse behavior to the yarn transverse behavior Cheng *et al.* (2004, 2005) and Cheng and Chen (2006) carried out a series of transverse-compression tests using single PPTA-type (specifically, Kevlar® KM2) fibers and attempted to derive a rate-independent non-linear pseudo-elastic-type material model.

Within this model, transverse loading and transverse unloading/reloading behaviors of the fibers are treated separately in order to account for the loading-induced damage/stress-softening.

Main objective

The main objective of the present study is to extend our prior molecular-type simulation work (Grujicic *et al.*, 2011a, b) in order to:

- provide insight into the behavior of PPTA fibers when subjected to transverse loading; and
- to reveal the role of various microstructural and topological molecular/fiber-level defects on the mechanical transverse response of PPTA.

While a large fraction of the ballistic/blast protective systems fabricated today are based on polymer matrix composites containing Kevlar® KM2 reinforcements, the present work will deal with generic PPTA fibers. In other words, while there are a number of specific Kevlar® and Twaron® grades of fibers, microstructure and properties of all these grades are believed to be dominated by their main PPTA constituent.

Paper organization

In Section 2, a brief overview is provided of the main experimental findings, reported in the open literature, pertaining to the mechanical transverse behavior of PPTA fibers. Details regarding the molecular-modeling techniques used including computational models, force-fields, computational algorithms and post-processing data-reduction analyses are presented in Section 3. The main results obtained are presented and discussed in Section 4, while the key findings resulting from the present work are summarized in Section 5.

2. Experimental transverse behavior of PPTA fibers

In this section, a comprehensive summary is provided of the main experimental findings dealing with the mechanical transverse behavior of PPTA fibers. Examination of the literature reveals that the majority of the experimental findings can be attributed to the work of Cheng *et al.* (2004, 2005), Cheng and Chen (2006) and Lim *et al.* (2011). In the remainder of this section, a brief summary is provided of the main findings obtained by Cheng *et al.* (2004, 2005), Cheng and Chen (2006) and Lim *et al.* (2011). For clarity, and to obtain a chronological perspective of the subject matter, the findings reported in the key papers of Chen and co-workers are presented separately.

2.1 Cheng et al. *(2004)*

Cheng *et al.* (2004) established and utilized an experimental setup to study the transverse mechanical properties of Kevlar® KM2 fibers. Their main findings can be summarized as follows:

(1) Under large transverse compressive strains, Kevlar® KM2 fibers display considerable material non-linearity.

(2) Material non-linearity has been found to result from the accumulation of deformation-induced damage which leads to stress-softening (a Mullins-effect-like phenomenon). Consequently, the primary loading and unloading paths are quite different, revealing a considerable amount of energy dissipation. As far as reloading is concerned, it is found to coincide with the unloading path until the maximum strain attained by the primary loading path is reached. Beyond this point, reloading path becomes an extension of the primary loading path.

(3) Longitudinal tensile load-bearing capacity of the fibers is only weakly affected by the presence of large transverse deformations.

(4) On the other hand, fiber transverse stiffness at large transverse strains is increased by the presence of longitudinal loads.

(5) Transverse mechanical behavior of the fibers is only weakly affected by the rate of deformation over the entire (large) strain range.

(6) Fiber transverse stiffness, as quantified by the transverse Young's modulus, is determined by:

- solving the plane strain problem associated with the fiber transverse compression in order to obtain a relationship between the transverse load and the transverse deflection while treating the fiber material as being transversely isotropic; and
- fitting the experimental data to this functional relationship using a non-linear regression procedure.

The resulting fiber transverse modulus was found to be 1.34 ± 0.35 GPa.

2.2 Cheng et al. *(2005)*

In Cheng *et al.* (2005) a more comprehensive mechanical testing program was employed to determine the behavior of single Kevlar® KM2 fibers under transverse, longitudinal and combined transverse/longitudinal loading conditions. The main findings obtained can be summarized as follows:

- Under longitudinal tensile loading conditions, both virgin fibers and the fibers pre-deformed transversely, behave as linear elastic materials with a mean failure strength of 3.88 ± 0.40 GPa and a mean failure strain of 4.52 ± 0.37 percent.
- Under tensile longitudinal loads, fibers generally fail in a fibrillation mode. Within this failure mode, fibrils fail transversely, causing the (failed) fiber ends to splinter.
- Under transverse compressive loading conditions, fibers, regardless of the presence/absence of longitudinal loading/strain, display the aforementioned material non-linearity, stress-softening, Mullins effect and strain-rate-insensitivity.
- The overall decoupling between the longitudinal and transverse responses of the fibers previously reported by Cheng *et al.* (2004) has been confirmed over a wide range of strains, strain rates and combined loading conditions.

2.3 Cheng and Chen (2006)

In Cheng and Chen (2006), the experimental results reported by Cheng *et al.* (2004, 2005) are used to derive and parameterize a phenomenological model which accounts for the observed behavior of Kevlar® KM2 single fibers under transverse compressive

loading conditions. The model developed is an adaptation of the continuum pseudo-elastic material model originally proposed by Holzapfel *et al.* (1999) which treats the same material as two different elastic materials depending on whether the loading takes place along the primary loading path or the material is being unloaded/elastically reloaded. This approach enables the inclusion of stress-softening and residual strain inelastic effects without the introduction of additional behavior-governing equations such as a yield criterion or a flow-rule relation. As far as the material-damage evolution equation is concerned, it is derived under the condition that the extent of damage scales with the maximum principal stretches experienced by the material over the entire prior loading history. On the other hand, stress vs principal stretch relation over the primary loading path is described using the conventional Ogden hyperelastic strain-energy function. The model is parameterized using the stress vs principal stretch experimental results obtained during the first loading/unloading cycle and validated by comparing the model predictions against the experimental stress vs principal stretch data corresponding to the subsequent loading cycles.

2.4 Lim et al. *(2011)*

The experimental investigation reported by Lim *et al.* (2011) included single PPTA fibers from the following grades: Kevlar®, Kevlar®129, and Twaron® fabricated at different times over a period of ten years. In addition, the investigation utilized a miniaturized tensile Kolsky bar to extend rates of deformation into the range generally encountered under ballistic-impact conditions. The results obtained could be summarized as follows:

- longitudinal tensile strength of the fibers is only weakly dependent on the fiber gage length, imposed loading rate and age of the fiber;
- under high deformation rates, transverse compression tends to lower the ultimate tensile longitudinal strength of the fibers, but only by a few percent; and
- over the entire loading rate range examined, the prevailing tensile longitudinal failure mode of the fibers is fibrillation.

Under these conditions, compressive transverse loading, as mentioned above, has relatively small effect on the fiber longitudinal tensile strength. However, in some situations, transverse compression can promote "cleavage-like" fiber failure in which case the tensile longitudinal strength can be substantially (by approximately 50 percent) reduced.

3. Molecular-level computational analysis

As mentioned earlier, molecular-level computational methods have been employed in the present work in order to obtain additional insight into the PPTA fiber transverse behavior and into the role various imperfections/defects play in this behavior. In general, the formulation of a molecular-level simulation problem requires, at a minimum, specification of the following five items:

(1) a molecular-level computational model consisting of atoms, ions, moieties and functional groups;

(2) a set of force-field functions, which describe various bonding and non-bonding interactions between the constituents of the molecular-scale model;

(3) types and sequence of the computational method(s) to be used in the simulation;

(4) formulation of the physical problem being investigated/simulated; and
(5) specification of the methods and procedures to be used in the post-processing data-reduction analysis.

A brief overview of these items is provided in the remainder of this section.

3.1 Computational model

To gain insight into transverse behavior of PPTA fibers, a relatively large number of molecular-level computational models containing various perfect-crystal PPTA conformations and different microstructural/topological defects were used in the present work. Figure 3 shows several examples of the computational models used. The models used were all constructed using Visualizer [I] and Amorphous Cell [II] molecular-microstructure pre-processing tools.

Construction of the defect-free PPTA computational material models was carried out under the following conditions:

(1) The fibers are treated as bundles of parallel fully crystalline fibrils.
(2) As far as the crystalline structure of the fibrils is concerned, it is modeled as a stack of parallel PPTA sheets (formed by hydrogen bonding between nearly-parallel PPTA molecular chains, all aligned in the fiber/fibril-axis direction).
(3) To account for the fact that the vast majority of the molecules inside PPTA fibrils are fully surrounded by other chains:
    - A bulk-like environment is created using the concept of the computational cell and the periodic boundary conditions. The computational cells used were all of the rectangular parallelepiped shape, with one of the computational-cell edges aligned with the fiber axis. The other two computational-cell edges lie in the PPTA sheet and orthogonal to it, respectively.
    - The periodic boundary conditions are applied not only in the fiber/fibril axial direction but also in the two transverse directions.
(4) Sheet pleating was not explicitly accounted-for since it occurs at a length scale exceeding the size of the PPTA computational cells used.

In the case of the computational cells containing imperfect crystalline PPTA, the following classes of crystallographic/topological defects were considered:

- chain ends (treated as point-type defects) terminated with one of the four possible end groups (—COOH, $-NH_2$, $-COO^-Na^+$, $-NH_3^+HSO_4^-$), Table I;
- side groups involving two possible moieties (—SO_3H, $-SO_3^-Na^+$), Table I;
- intra-fibril voids and interstitial H_2SO_4; and
- defect bands.

Defects are created within the initially perfect crystalline material by using the following procedures:

- chain scission followed by the attachment of the appropriate chain end groups, in the case of chain end defects;
- chain-side functionalization, in the case of side group defects;

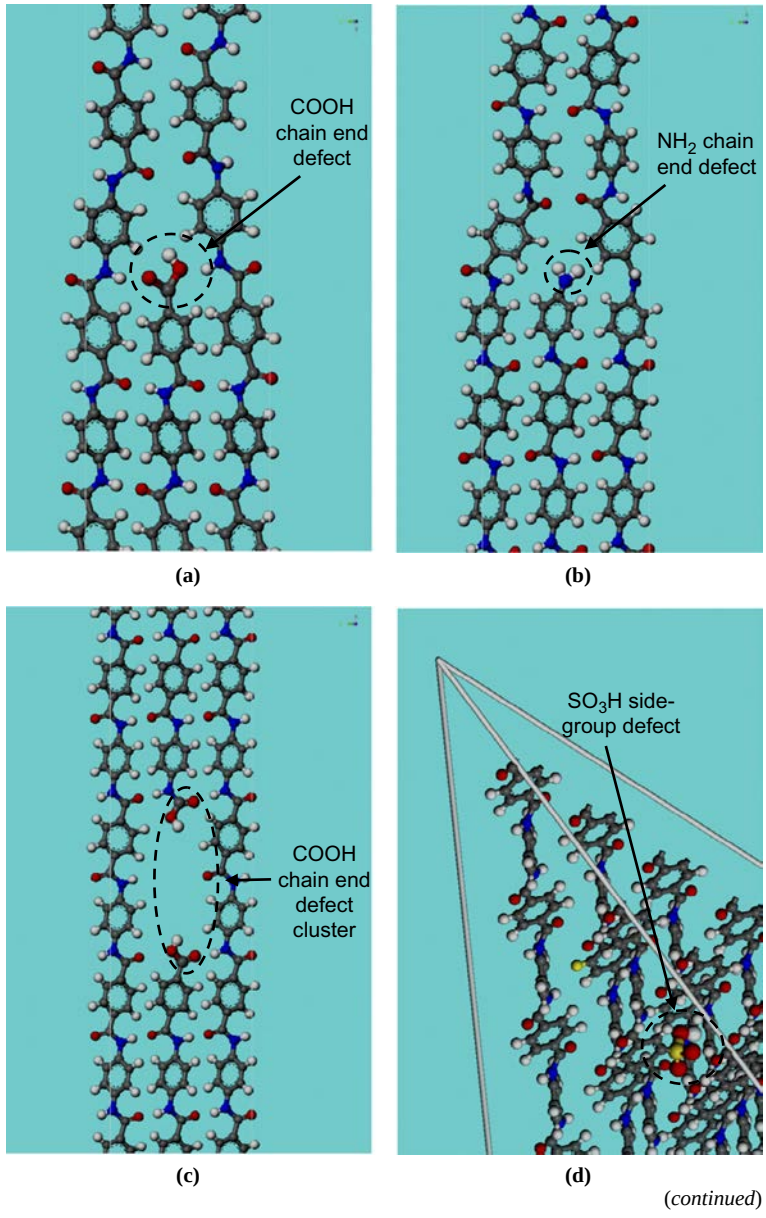

Figure 3.
Examples of the molecular-level computational models used to investigate

(*continued*)

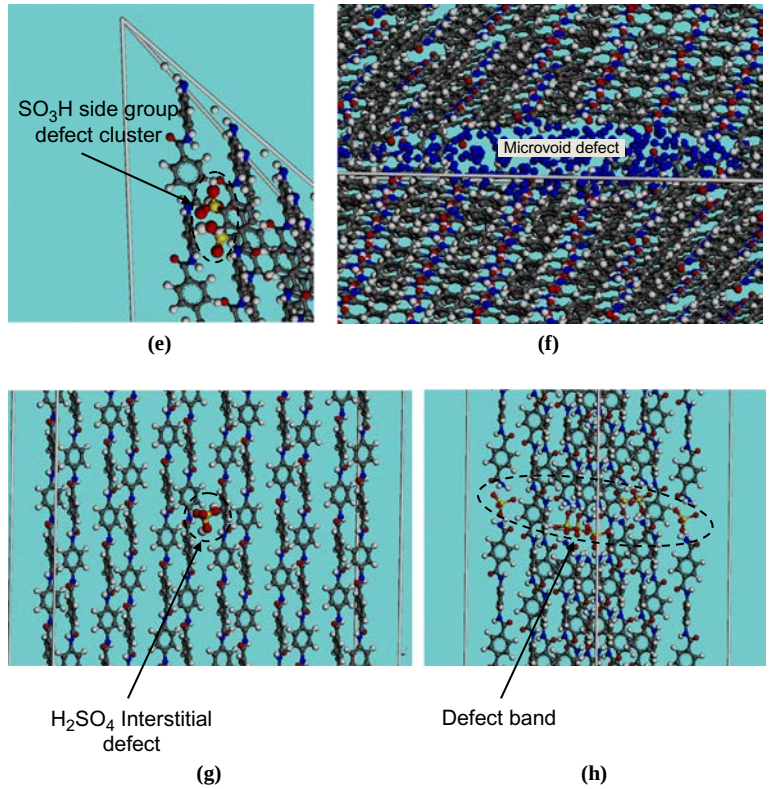

Notes: (a) A COOH chain-end defect; (b) a NH_2 chain-end defect; (c) a COOH chain-end defect cluster; (d) a SO_3H side-group defect; (e) a SO_3H side-group defect cluster; (f) a microvoid defect; (g) a H_2SO_4 interstitial defect; and (h) a collection of chain ends forming a defect band

Figure 3.

- insertion of nitrogen molecules, in the case of (air-filled) voids;
- insertion of H_2SO_4 molecules, in the case of interstitials; and
- scission of a number of adjacent chains in a plane orthogonal to the fibril axis, in the case of defect bands.

Additional details regarding the molecular-level microstructures and topologies associated with each of these defects could be found in our prior work (Grujicic *et al.*, 2011a, b).

3.2 Force-fields

As mentioned earlier, the behavior of a material system at the molecular-level is governed by the appropriate force-fields which define functional relationships between different components of the constituent-particle (atom/ion) interaction energies and the particle position, nature, charge, and state of bonding. In the present work, the so-called condensed-phase optimized molecular potentials for atomistic simulation studies (COMPASS) force-field is used (Sun, 1998; Sun *et al.*, 1998). This highly accurate

force-field is of an *ab initio* type since most of its parameters were determined by matching the predictions made by the *ab initio* quantum mechanics calculations to the condensed-matter experimental data. Within this force-field, the potential energy of a system of interacting atoms/ions is expressed as a sum of a valence (covalent-bonding) term, a cross (atomic-environment-dependent bonding) term, and a non-bond van der Waals and Coulombic (including hydrogen-bonding) pair-interaction term. A summary of the COMPASS force-field functional relations can be found in our previous work (Grujicic and Lai, 1999; Grujicic *et al.*, 2004).

3.3 Computational method

To gain insight into the mechanical response of a perfect and defective crystalline PPTA, computational cells described earlier were subjected to molecular statics and molecular dynamics simulations. The molecular statics approach is effectively an optimization procedure within which the potential energy of the computational-cell (the objective function) is minimized with respect to the positions of the constituent atoms and ions (the design variables). The potential energy minimization within Discover (Materials Studio, 2009) (the atomic simulation program from Accelrys used in the present work) is carried out by applying sequentially several minimization algorithms in order to attain an optimal combination of computational efficiency and robustness.

Within the molecular dynamics approach, the following two-step procedure is repeated at each (0.1-1.0 fs long) time step:

(1) the negative gradient of the potential energy with respect to the atom/ion positions is first used to compute forces acting on each atom/ion; and

(2) then, the associated Newton's equations of motion are integrated numerically in order to compute the acceleration associated with each atom/ion and to, in turn, update the velocity and the position of each atom/ion.

To ensure that the system is in a state of equilibrium and is not subjected to any thermodynamic/mechanical fluxes, only equilibrium molecular dynamics methods were used in the present work. Within these methods, the system of interacting atoms/ions under consideration is coupled to a (infinite-extent, external) surrounding (e.g. a constant temperature reservoir, in the present case). In the present work, NVT equilibrium molecular dynamics simulations are employed (where N is the (fixed) number of atoms/ions within the computational cell, V is the computational cell volume (also fixed), and T (= 298 K) is the fixed temperature).

3.4 Problem formulation

As mentioned earlier, the problem analyzed in the present work involves the mechanical response of PPTA fibers subjected to transverse compressive loading. Typically, PPTA fiber diameter is on the order of 10 μm, a length scale which is 10^3-10^4 times larger than the size of a prototypical molecular-level computational cell. As established earlier, fibers are composed of parallel crystalline fibrils with lateral dimensions being one to two orders of magnitude smaller than those of the fibers. Taking these findings into consideration, it is clear that a PPTA material domain of the size equal to that of the computational cell has the highest probability of residing within a single PPTA fibril. That is the reason that, within the present work, all the computational cells are assumed to be perfect or imperfect single-crystalline.

Considering the above, the problem analyzed within the present work involves simple uniaxial compression of different computational cells in each of two transverse directions (one direction at a time). The compression is carried out in small increments and each incremental compression is followed by the computational cell energy-minimization and extended (ca. 40 ns) molecular-dynamics simulation runs. The results obtained are post-processed using the procedures described in the next section in order to establish compressive stress vs transverse stretch relations. In addition, deformed microstructure is examined in great detail in order to identify the nature of inelastic deformation processes responsible for the experimentally-observed stress-softening and residual strain effects.

The aforementioned procedure for incremental transverse loading, including molecular static, energy-minimization and prolonged molecular-dynamics-based thermal equilibration, is conducted through the use of a Discover input file (Materials Studio, 2009). This file is written using the Basic Tool Command Language (BTCL) which enabled the use of a scripting engine that provides very precise control of simulation tasks.

3.5 Post-processing data-reduction analysis

As mentioned earlier, the main purpose for the extensive use of molecular-level computational analyses in the present work was to assess PPTA fibril/fiber transverse mechanical properties and their dependence on the type, size and concentration of various microstructural/topological defects. The main mechanical properties considered in the present work include material stiffness and strength. The post-processing data reduction procedures used to determine these PPTA fibril/fiber mechanical properties from the molecular-level computational results are described in the remainder of this section.

3.5.1 Elastic stiffness. Within the molecular-level computational framework, molecular statics and/or molecular dynamics approaches can be used to determine the components of the fourth-order elastic stiffness tensor. When molecular statics approaches are used, the contributions of the finite-temperature thermal expansion and the vibrational/configurational entropic effects to the system free energy are ignored. Consequently, the resulting elastic stiffness tensor defined as a second-order derivative of the system's free energy (i.e. potential energy, in the zero temperature case) with respect to the unit-cell strain components reflects the behavior of the material in question under small deformations at zero absolute temperature. Since these finite-temperature effects can make a significant contribution to the elastic stiffness tensor, they could not be generally neglected. Consequently, a molecular-dynamics-based elastic-stiffness computational procedure which accounts for the aforementioned thermal and entropic effects is utilized in the present work. A brief description of this procedure is provided in the remainder of this section. However, before describing this procedure, it should be recalled that the three principal (i.e. computational-cell edge) directions are, respectively, aligned with:

(1) the fibril/fiber longitudinal direction, direction x_1;

(2) with the sheet-normal direction, direction x_2; and

(3) with the corresponding in-sheet orthogonal direction, direction x_3.

Within the approach used, the elastic stiffness tensor is determined using the prolonged equilibrium molecular dynamics simulation results to calculate the

time-based correlation functions between different stress and strain components. The components of the strain, ε_{ik}, and stress, σ_{nj}, second-order tensors are calculated, respectively, as:

$$\varepsilon_{ik} = \frac{1}{2}\left(h_{nl}\langle h\rangle_{lk}^{-1} h_{np}\langle h\rangle_{pi}^{-1} - \delta_{ik}\right) \tag{1}$$

$$\sigma_{nj} = \frac{1}{V}\left\{\sum_{a}\frac{(p_a)_n(p_a)_j}{m_a} + \sum_{a>b}\frac{\partial U}{\partial r_{ab}}\frac{(x_{ab})_n(x_{ab})_j}{r_{ab}}\right\} \tag{2}$$

where h_{ij} is an (i, j) element of a second-order tensor defining the three unit cell edge-vectors within the reference frame, δ_{ij} is the Kronecker delta, V is the computational-cell volume, p_a is the momentum of atom a, m_a is the mass of atom a, U denotes the potential energy function, r the inter-particle spacing, x the inter-particle position vector, and angular brackets are used to denote the time/ensemble average of a given quantity.

The components of the elastic stiffness fourth-order tensor, C, are next computed using the following equations:

$$C_{iklm} = \frac{k_B T}{\langle V\rangle}\langle\varepsilon_{ik}\varepsilon_{lm}\rangle^{-1} \tag{3}$$

or:

$$C_{iklm} = \langle\varepsilon_{ik}\sigma_{nj}\rangle\langle\varepsilon_{nj}\varepsilon_{lm}\rangle^{-1} \tag{4}$$

where k_B is the Boltzmann's constant, T is the absolute temperature, and $\langle a_{ik}b_{lm}\rangle$ is the time-based correlation function between the (i, k)-component of a second-order tensor a and the (l, m)-component of a second-order tensor b.

The fourth-order elastic stiffness tensor C_{iklm} is then converted, using the Voigt notation, into a 6×6 elastic stiffness matrix, C. The results obtained in the present work generally showed that the C matrix contains nine independent elements, suggesting that the PPTA crystal structure possesses orthotropic symmetry.

Since it is customary practice to work with the engineering moduli rather than with the elastic stiffness constants, the corresponding three Young's moduli (E_{11}, E_{22}, E_{33}), three shear moduli (G_{12}, G_{13}, G_{23}), and three Poisson's ratios ν_{12} ($= \nu_{21}{}^{*}E_{11}/E_{22}$), ν_{13} ($= \nu_{31}{}^{*}E_{11}/E_{33}$) and ν_{23} ($= \nu_{32}{}^{*}E_{22}/E_{33}$), are next determined using standard functional relations (Grujicic *et al.*, 2010a).

3.5.2 Strengths. Tensile and compressive strengths in three orthogonal (principal) directions are determined by subjecting the unit cell to the appropriate deformation mode and by monitoring the corresponding stress component. The mathematical procedure used to calculate stress components within a molecular length-scale framework was presented in the previous section, equation (2). In the case of tensile strengths, this strength component is set equal to the corresponding stress-component value at which the rate of stress increase with increase in strain begins to decline appreciably (denoting the onset of inelastic deformation). On the other hand, in the case of compressive strengths, the corresponding stress component is typically found to increase monotonically with strain. Consequently, the material compressive strength at a given strain level is set equal to the value of the corresponding stress component.

4. Results and discussion

In this section, the results of the molecular-level computational analyses used to assess transverse mechanical properties of the PPTA fibers are presented and discussed. In addition, a few results pertaining to the longitudinal mechanical response of PPTA fibers are also presented merely to demonstrate the capabilities of the present computational procedure and to ensure its validity (through comparison of the computed and experimental results).

Before the results are presented and discussed, it is important to establish a geometrical/kinematic relationship between the computational cells utilized in the present work and a typical PPTA fibril/fiber/yarn architectural hierarchy. This relationship is schematically shown in Figure 4(a)-(c). In Figure 4(a), a schematic of a prototypical PPTA computational cell used in the present work is depicted. As mentioned earlier, the material region covered by the computational cell is assumed to reside within a single PPTA fibril. As seen in Figure 4(b), which depicts a single PPTA fiber, such a fiber consists of a number of nearly parallel fibrils. Within each of the fibrils, the fibril axis lies within the PPTA sheets and the fibrils merely differ in the orientation of the sheet normals (the sheet normal in each fibril is orthogonal to the fibril/fiber axis). Figure 4(c) displays the typical kinematic relationship between the fibers and the yarns. Simply stated, the yarns are treated as assemblies of nearly parallel fibers which are given a light twist in order to mechanically engage the fibers.

Based on the computational-cell/fibril/fiber/yarn kinematic relationship shown in Figure 4(a)-(c), it is clear that the present computational analysis can only yield

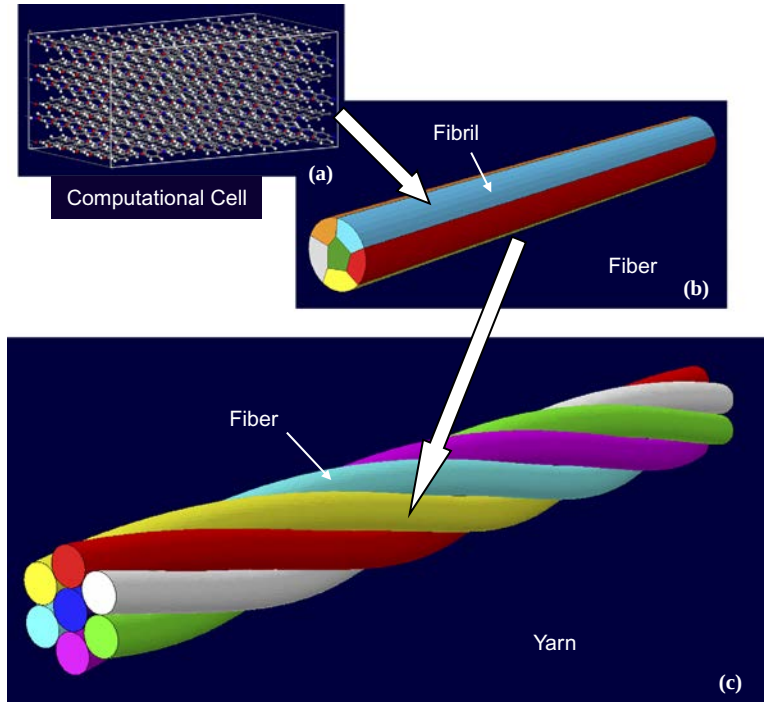

Figure 4.
Topological relationships between: (a) a prototypical PPTA computational cell used in the present work; (b) PPTA fibrils within a single fiber; and (c) multi-fiber lightly-twisted yarns

(orientation-dependent) mechanical properties of the fibrils. Hence, to obtain the corresponding fiber and yarn mechanical properties, averaging/homogenization methods should be employed and, in the case of yarns, consideration should be given to additional phenomena such as inter-fiber contacts and friction. While determination of the yarn effective mechanical properties is beyond the scope of the present work, examples of the procedures used in such determination can be found in our prior work (Grujicic *et al.*, 2011b).

4.1 Mechanical properties of PPTA fibrils

As established earlier, since the computational cells utilized reside within the fibrils, the results obtained reveal the mechanical properties of the fibrils. It should be recalled that in the present investigation, both the computational cells containing perfectly crystalline and defective PPTA were analyzed, which enables quantification of the effects of various microstructural/topological defects on the fibril mechanical properties (via the use of the procedures described in Subsection 3.5). It should also be noted that there are several reports of experimentally-examined mechanical properties of PPTA fibrils. Among these, the ones most noteworthy are the works of Konopasek and Hearle (1977), Morgan *et al.* (1983), Panar *et al.* (1983), Dobb *et al.* (1977, 1981) and Hearle *et al.* (1989).

4.1.1 Stiffness of PPTA fibrils. As expected, the present computational procedure clearly revealed that the fibril stiffness is affected by the type, size, concentration/number density and clustering of microstructural/topological defects. Examples of the typical results obtained in this portion of the work are shown in Figures 5(a)-(d), 6(a)-(b) and 7(a)-(c). Figure 5(a)-(d) shows, respectively, the effect of the concentration of the —COOH, $—NH_2$, $—SO_3H$ and $NH_3^+HSO_4^-$ chain-end groups on the relative change in the nine orthotropic elastic moduli with respect to their values in the defect-free fibrils ($E_{11} = 105.3$ GPa, $E_{22} = 2.0$ GPa, $E_{33} = 31.3$ GPa, $G_{12} = 0.9$ GPa, $G_{13} = 5.6$ GPa, $G_{23} = 2.6$ GPa, $\nu_{12} = 0.46$, $\nu_{13} = 0.147$ and $\nu_{23} = 0.15$). The effect of the concentration of the $—SO_3H$ and the $SO_3^-Na^+$ side groups on the orthotropic elastic constants is shown in Figure 6(a) and (b), respectively. The effect of the concentration of the voids and the mobile H_2SO_4 molecules on the same set of elastic constants is shown in Figure 7(a)-(c), respectively.

Examination of Figures 5(a)-(d), 6(a)-(b) and 7(a)-(c) reveals that:

- The orthotropic elastic constants change monotonically with an increase in the defect concentrations.
- Among the elastic constants, longitudinal normal stiffness (E_{11}) and the inter-sheet shear stiffness (G_{12}) are most strongly affected/compromised by the presence of the chain-end defects, Figure 5(a)-(d).
- In the case of side-group defects, Figure 6(a) and (b), trans-sheet normal stiffness increases either strongly due to establishment of inter-sheet hydrogen bonds (the case of SO_3H, Figure 6(a)), or weakly if such hydrogen-bonding is absent (the case of $SO_3^-Na^+$, Figure 6(b)). Figures 6(a) and (b) further reveal that the shear moduli G_{12} and G_{13} are also increased due to the presence of hydrogen bonding.
- The presence of voids and interstitial defects has a highly detrimental longitudinal stiffness reducing effect, Figure 7(a) and (b).

This effect is even more pronounced in the case of defect bands, Figure 7(c).

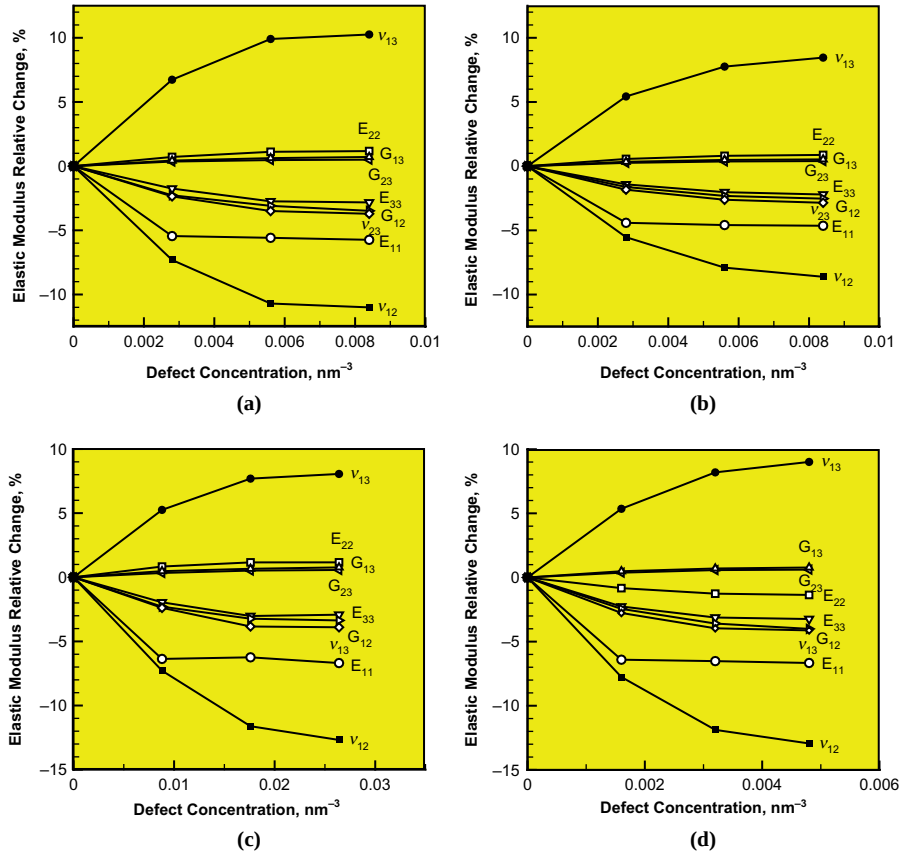

Figure 5.
The effect of the concentration of the: (a) —COOH; (b) —NH_2; (c) —COO^-Na^+; and (d) $NH_3^+HSO_4^-$ chain end groups on the orthotropic elastic stiffness constants of the PPTA fibrils

To predict the mean values of the orthotropic elastic constants in fibrils of the commercially produced PPTA fibers, the following deterministic procedure was employed:

- For each of the microstructural/topological defects analyzed in the present work, a mean value of the defect concentration (and its typical range) under prototypical PPTA-fiber fabrication conditions is assessed using the available open-literature reports. More detailed description of this assessment procedure can be found in our prior work (Grujicic *et al.*, 2011b).
- Due to the very low values of the defect concentrations, it is assumed that the combined effects of different defects can be obtained using a simple linear-superposition procedure.
- The effect of individual defects on the fibril orthotropic elastic constant *s* is assumed to be represented by the results shown in Figures 5(a)-(d), 6(a)-(b) and 7(a)-(c).

It should be noted that the mechanical properties (including elastic stiffness) of the individual PPTA fibrils are not generally experimentally measured and the relevant data are not available in the open literature. Instead, single fibers are often tested and

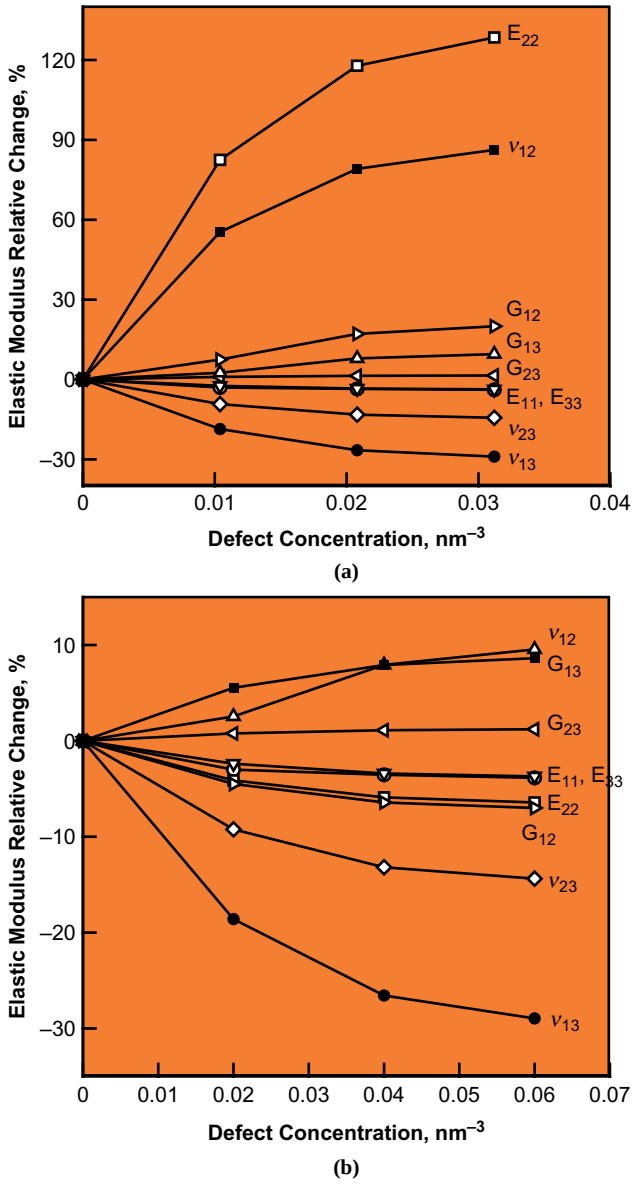

Figure 6.
The effect of the concentration of the: (a) $-SO_3H$ and (b) $SO_3^-Na^+$ side groups on the orthotropic elastic constants of the PPTA fibrils

the fiber mechanical-property data are available. It should be recalled that the longitudinal axes of the fibrils and the fiber are effectively coincident and, hence, one expects that the fibril longitudinal properties are fairly representative of the fiber longitudinal properties. In other words, to provide the grounds for validation of the present computational model, computed longitudinal Young's modulus E_{11} ($= 105.3 \pm 5.3$ GPa) is compared with its experimental fiber-based counterpart

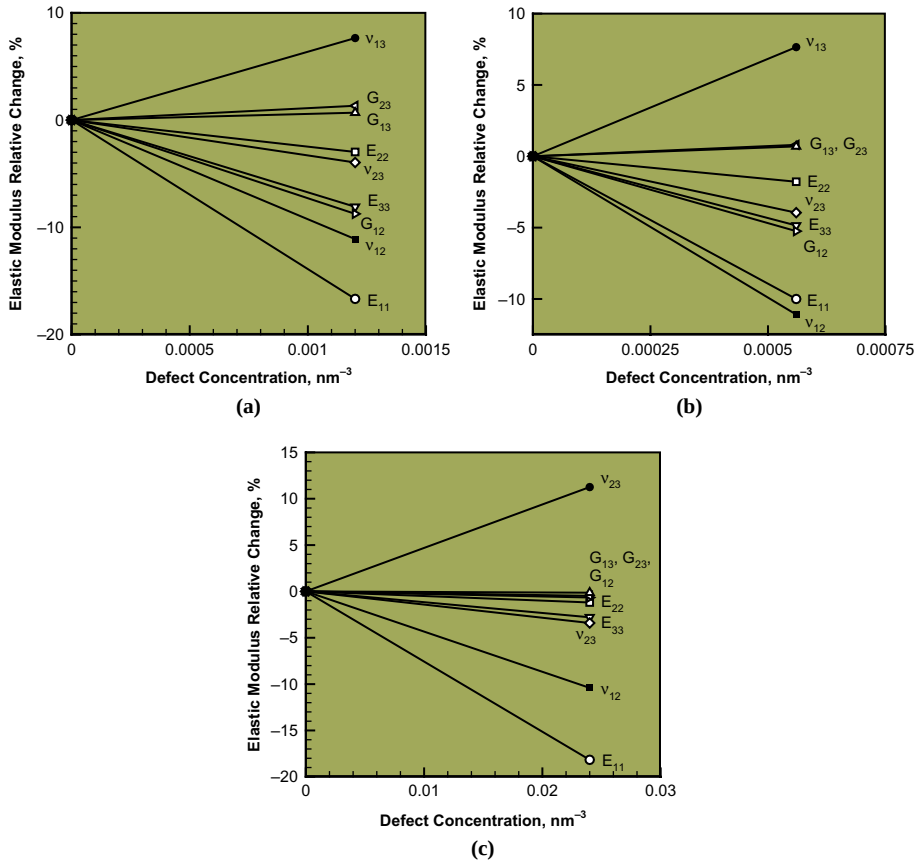

Figure 7.
The effect of the concentration of the: (a) voids; (b) mobile H_2SO_4 molecules; and (c) defect bands on the orthotropic elastic constants of the PPTA fibrils

(= 84.62 ± 4.18 GPa) (Cheng *et al.*, 2004). This comparison suggests that the present computational analysis reasonably well accounts for the longitudinal stiffness behavior of the PPTA fibrils/fibers. As far as the PPTA fiber transverse stiffness is concerned, it is also generally measured (Cheng *et al.*, 2004). However, since in the transverse direction, fibrils can have a variety of crystallographic orientations, a direct comparison between the fibril and fiber transverse stiffnesses is not possible. Instead, one has to first apply an averaging/homogenization procedure to the fibril transverse stiffness in order to compute an "effective" transverse stiffness for the fiber. Then, a computation/experiment comparison regarding the fiber transverse-stiffness properties can be carried out. In the present work, two averaging schemes were applied:

(1) a constant-strain upper bound Voigt averaging scheme; and

(2) a constant-stress lower bound Reuss averaging scheme.

The two averaging schemes yielded 2.9-6.5 GPa range for the PPTA fibril/fiber transverse Young's modulus. This range is in fair agreement with its experimental counterpart $E_{11} = 1.34 \pm 0.35$ GPa (Cheng *et al.*, 2004).

4.1.2 Fibril strength.

Fibril longitudinal strength. The procedure for calculation of the fibril longitudinal strength was developed in our recent work (Grujicic *et al.*, 2011b). This procedure established the following:

(1) The fibril compressive strength is controlled by buckling. Since buckling-controlled compressive strength is, in general, significantly lower than the material compressive strength, the material compressive strength determined using the computational procedures described in Section 3.5 is of limited use.

(2) On the other hand, the procedure described in Section 3.5 can be used to compute the fibril/fiber longitudinal tensile strength. This procedure, in the case of perfectly crystalline PPTA, yielded the fibril/fiber tensile longitudinal strength of approximately 6.3 GPa.

(3) The results obtained by Grujicic *et al.* (2011b) as well as the results obtained in the present work reveal that the fibril longitudinal tensile strength is effectively controlled by the size and composition of the largest (i.e. the most potent) defect cluster.

(4) Due to the stochastic character of the defects present within the fibrils, fibril/fiber longitudinal strength has been found to be also a stochastic quantity which is in agreement with several experimental reports (Newell and Sagendorf, 1999; Steenbakkers and Wagner, 1988; Knoff, 1987).

(5) By:

- assuming defect distribution within the fibrils follows the principles of a Poisson point process;
- introducing the concept of "volume of influence" in order to establish a criterion for declaring an ensemble of closely-spaced individual defects a single (high potency) defect cluster;
- using the defect concentrations associated with the prototypical PPTA fiber fabrication conditions;
- using the results of the molecular-level calculations; and
- carrying out an exercise in statistical probability analysis, a probability distribution function for the longitudinal strength of PPTA fibrils was derived and parameterized by Grujicic *et al.* (2011b).

Application of this procedure to the results obtained in the present work yielded the PPTA fibril/fiber longitudinal tensile strength probability density and cumulative probability density functions depicted, respectively, in Figure 8(a) and (b). Examination of the results displayed in these figures and the fact that the measured PPTA-fibril longitudinal tensile strength is typically found to be in a 3-5 GPa range (Cheng *et al.*, 2004; Newell and Sagendorf, 1999), suggests that the present computational procedure can reasonably well account for the experimental observations regarding the PPTA fibril/fiber longitudinal tensile strength. The cumulative distribution function shown in Figure 8(b) defines the probability that the PPTA fibril/fiber longitudinal tensile strength is lower than a given value and this type of function is often used in probabilistic/reliability-based design analyses (Grujicic *et al.*, 2006, 2010b).

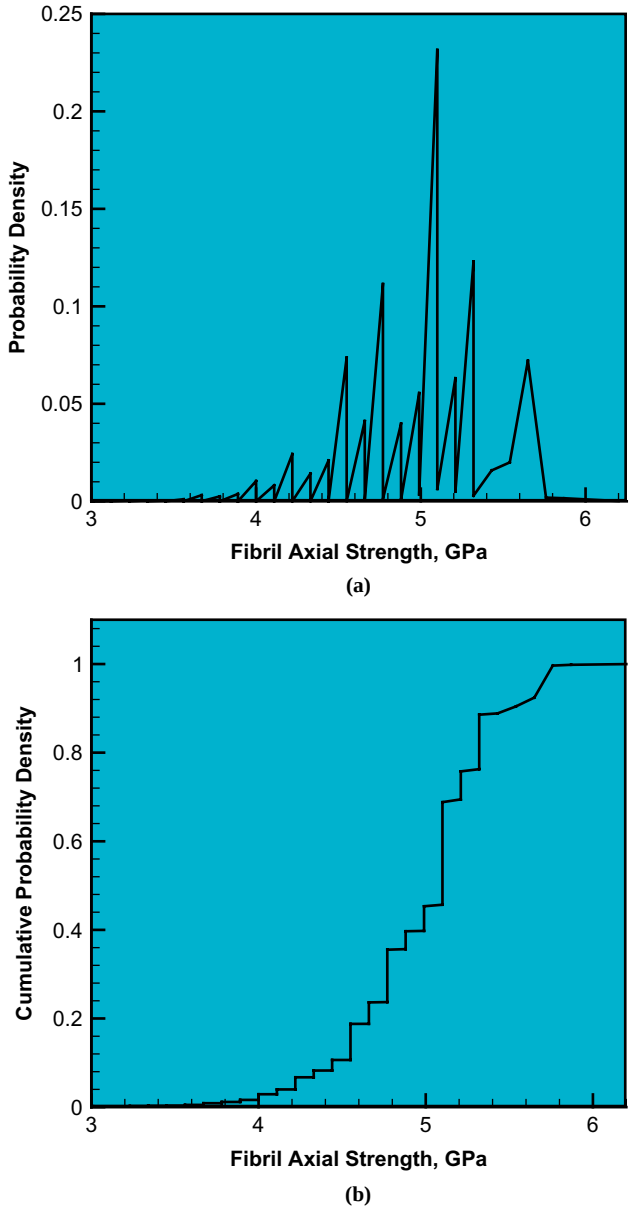

Figure 8.
(a) PPTA-fibril longitudinal-strength probability density function and (b) the corresponding cumulative distribution function determined in the present work using molecular-type computational analyses

Fibril transverse strength. To determine the transverse compressive strength of PPTA fibrils, both the unit cell containing the "perfect" PPTA crystal structure and the ones containing "defective" PPTA structures have been tested in compression. Compression has been applied both in the x_2 direction (corresponding to the case when the PPTA sheets are loaded "edge-on") and in the x_3 direction (the case in which the PPTA sheets'

normal is coincident with the compression direction). Since the results obtained are substantially different for the "edge-on" compression mode and for the normal compression mode, they are first presented and discussed separately. Then, the two sets of results are combined to obtain an effective transverse compressive strength of the PPTA fibrils.

Before the computational results obtained in this portion of the work are presented and discussed, however, it is important to briefly overview the corresponding experimental results. Figure 9 shows prototypical compressive transverse stress vs transverse stretch curves for a single Kevlar® KM2 fiber during a set of six load-unload-reload cycles (Cheng *et al.*, 2004). The salient features of this curve can be summarized as follows:

- The loading and the unloading paths are very different.
- Upon full unloading, a considerable fraction of the deformation remains unrecovered.
- Reloading, as long as it does not exceed the largest stress value ever attained during "primary" loading, takes place along the unloading path. Otherwise, reloading continues along the primary loading path.
- Primary loading is associated mainly with a concave-upward stress vs stretch functional relationship.

Edge-on compression. Examples of the computed edge-on compressive transverse stress vs transverse stretch curves for the perfect PPTA and defective PPTA fibrils are depicted, respectively, in Figure 10(a) and (b). Specifically, the results shown in Figure 10(b) correspond to the cases of a single, pair and triplet SO_3H side-group

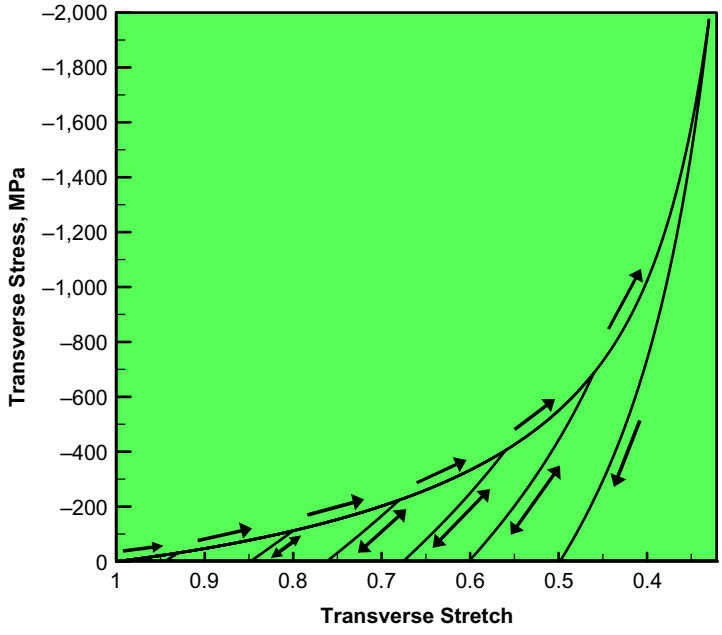

Figure 9.
Experimental results pertaining to the compressive transverse stress vs transverse stretch data for a single Kevlar® KM2 fiber as reported by Cheng *et al.* (2004)

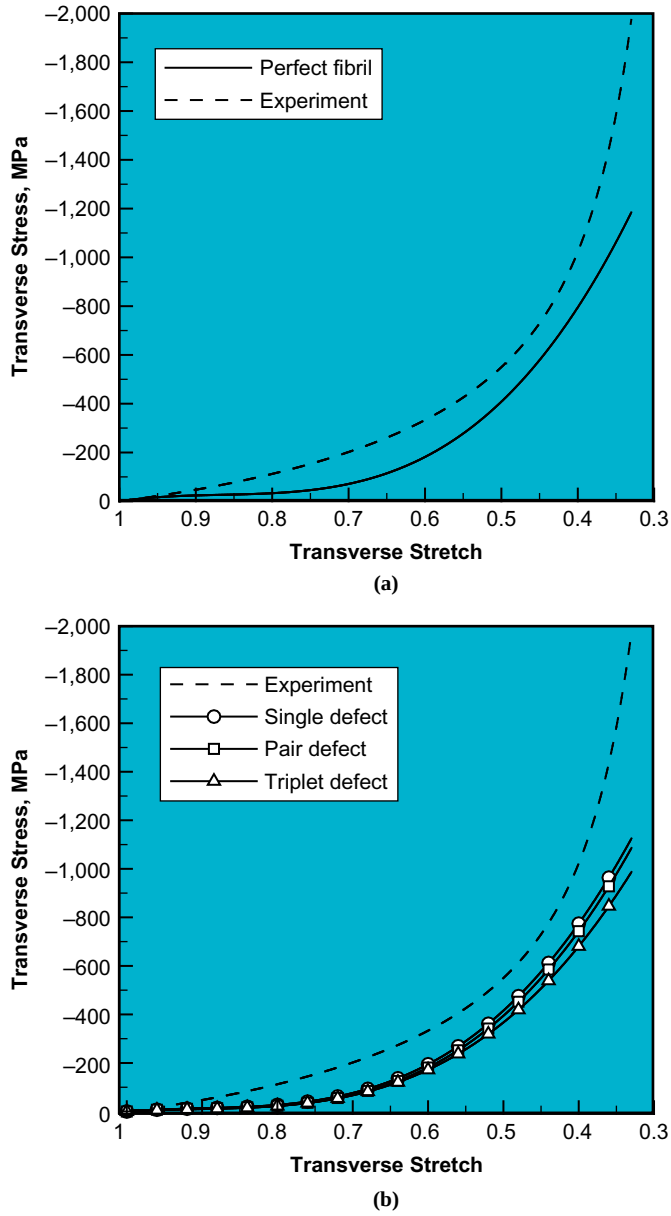

Figure 10.
Computed results pertaining to the edge-on compressive transverse stress vs transverse stretch data for a PPTA fibril with: (a) a perfect crystal structure and (b) defective crystal structures based on the presence of either a single SO_3H side-group defect, a SO_3H side-group pair or a SO_3H side-group triplet

defects (one defect cluster per computational cell). A comparison of the results shown in Figure 10(a) and (b) that the compressive edge-on transverse stress vs transverse stretch curve is greatly affected by the presence and size/clustering of microstructural/topological defects. Other results, not shown for brevity, reveal that the class (e.g. chain-end vs side-group) of defects also plays an important role.

In general, particularly at the lower levels of transverse deformation, the presence of defects can substantially (i.e. by more than 50 percent) reduce the transverse compressive strength relative to its level in the perfect PPTA fibrils. At the largest levels of transverse compressive deformation, the presence of defects has a somewhat smaller detrimental effect on the fibril transverse strength.

Temporal evolution of the molecular-level microstructure within a stack of PPTA sheets during edge-on compression of a perfect PPTA fibril is shown in Figure 11(a)-(d). Examination of the results displayed in these figures shows clear evidence of wall buckling under the applied compressive loading. In all the cases analyzed, the buckled structure attains the state of a metastable equilibrium during loading and, thus, does not recover to the initially "perfect" PPTA crystal structure upon unloading. This finding may be correlated with the previously mentioned experimental observations regarding the operation of inelastic-deformation processes during transverse loading.

Temporal evolution of the molecular-level microstructure within a stack of PPTA sheets during edge-on compression of a defective PPTA fibril containing a single SO_3H

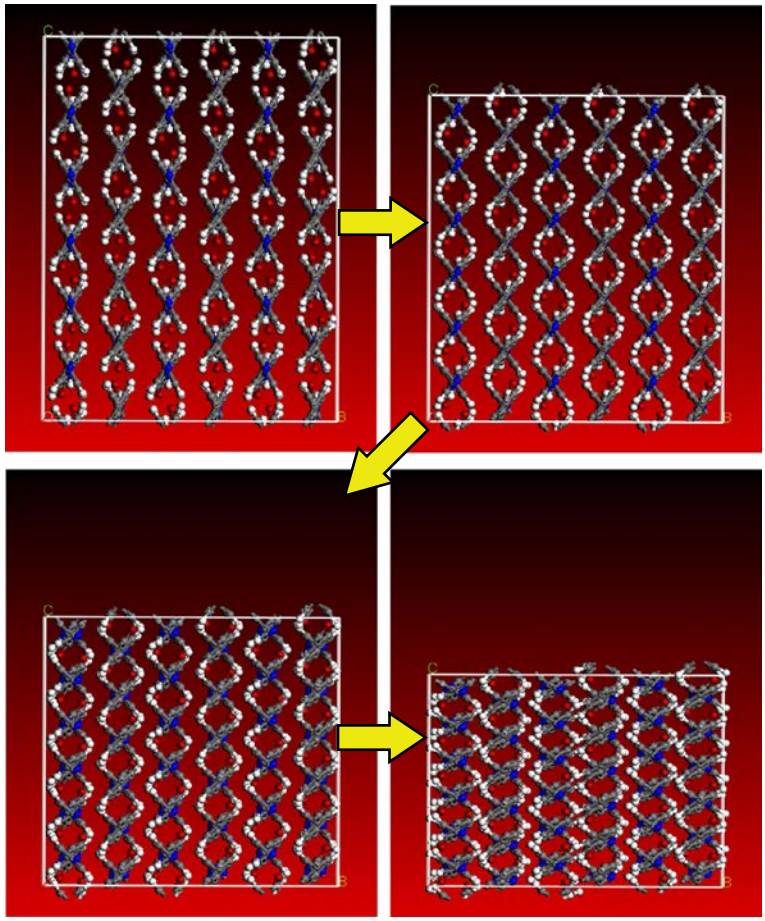

Figure 11.
Temporal evolution of a multi-sheet molecular-level microstructure during edge-on compression of a perfectly crystalline PPTA fibril

side-group defect is shown in Figure 12(a)-(d). It should be noted that the results shown in Figures 11(a)-(d) and 12(a)-(d) are generated at the same corresponding levels of the transverse stretch. Examination of the results shown in Figure 12(a)-(d), and their comparison with the corresponding results shown in Figure 11(a)-(d), reveals that the presence of defects facilitates the aforementioned sheet buckling (i.e. this process begins at the lower level of transverse deformation and takes place to a larger extent).

Normal compression. Examples of the computed normal compressive transverse stress vs transverse stretch curves for the perfect PPTA and defective PPTA fibrils are depicted, respectively, in Figure 13(a) and (b). As with Figure 10(b), the results shown in Figure 13(b) pertain to the cases of a single, pair and triplet SO_3H side-group defects. A comparison of the results shown in Figure 13(a) with the results shown in Figure 13(b), and subsequent comparison of these results with Figure 10(a) and (b) reveals that:

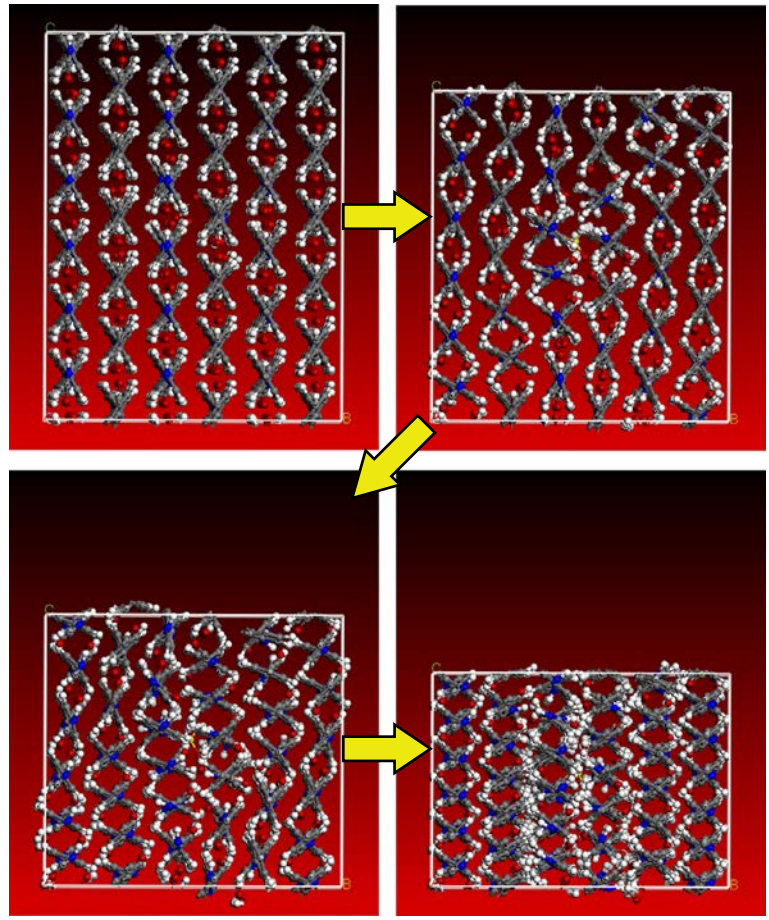

Figure 12.
Temporal evolution of a multi-sheet molecular-level microstructure during edge-on compression of a PPTA fibril containing a single SO_3H side-group defect per computational cell

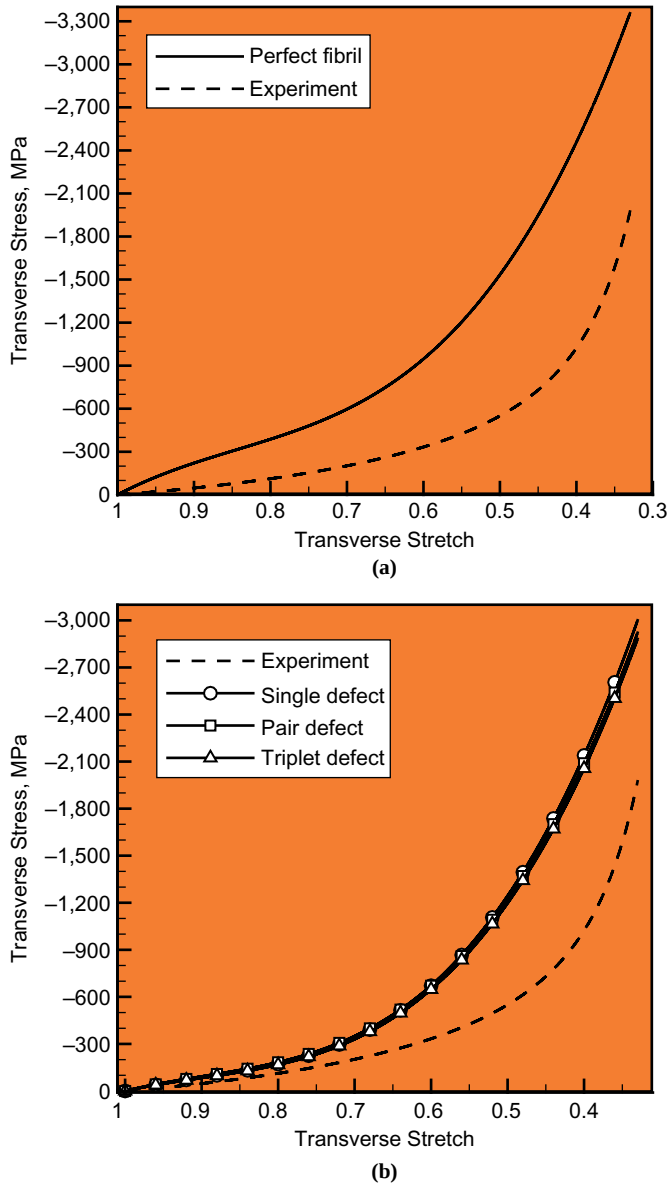

Figure 13.
Computed results pertaining to the normal compressive transverse stress vs transverse stretch data for a PPTA fibril with: (a) a perfect crystal structure and (b) defective crystal structures based on the presence of either a single SO_3H side-group defect, a SO_3H side-group pair or a SO_3H side-group triplet

- as in the case of edge-on compression, the compressive normal transverse stress vs transverse stretch curve is greatly affected by the presence and size/clustering of microstructural/topological defects;
- at the same level of the transverse stretch, the normal compressive transverse strength of both the perfect and defective PPTA fibrils is substantially higher (by ca. 200-300 percent) than the edge-on compressive transverse strength; and

- the compressive normal transverse stress vs transverse stretch curve is associated with a lower level of relative curvature suggesting that the deformation of the PPTA fibrils, in the present case, is dominated by (linear and non-linear) elastic deformations.

Temporal evolution of the molecular-level microstructure within a stack of PPTA sheets during normal compression of a perfect PPTA fibril is shown in Figure 14(a)-(d). Examination of the results displayed in these figures shows clear evidence that the sheet structure is maintained during normal compressive loading.

Temporal evolution of the molecular-level microstructure within a stack of PPTA sheets during normal compression of a defective PPTA fibril containing a single SO_3H

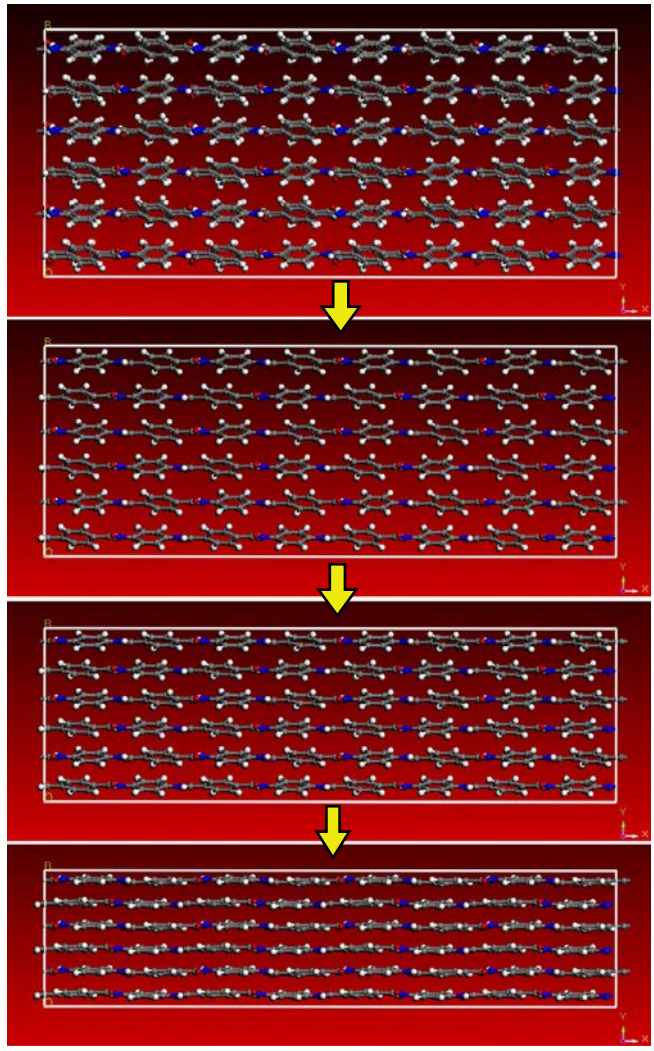

Figure 14.
Temporal evolution of a multi-sheet molecular-level microstructure during normal compression of a perfectly crystalline PPTA fibril

side-group defect is shown in Figure 15(a)-(d). It should be noted that the results shown in Figures 14(a)-(d) and 15(a)-(d) are generated at the same corresponding levels of the transverse stretch. Examination of the results shown in Figure 15(a)-(d), and their comparison with the corresponding results shown in Figure 14(a)-(d), reveals that the presence of defects causes undulations in the PPTA sheet structure and the magnitude of these undulations becomes somewhat reduced in the course of normal compressive loading.

Fibril effective transverse strength. The results shown in Figures 10(a)-(b) and 13(a)-(b) clearly reveal that the transverse compressive strength of PPTA fibrils is strongly dependent on the crystallographic character of the transverse loading direction. Since, during transverse compressive testing of single PPTA fibers a large number of PPTA fibrils is being subjected to the compressive loading, it is beneficial to derive a PPTA fibril effective transverse compressive strength by employing the

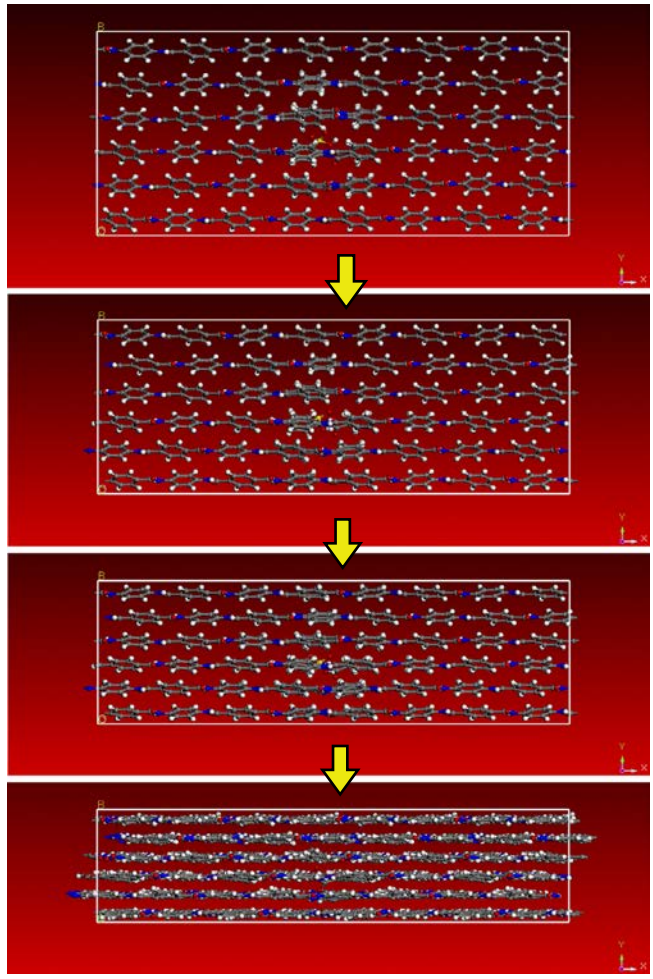

Figure 15.
Temporal evolution of a multi-sheet molecular-level microstructure during normal compression of a PPTA fibril containing a single SO_3H side-group defect per computational cell

previously mentioned Voigt and Reuss averaging procedures. In addition, for each lateral or transverse orientation of the fibril, an average transverse compressive strength needs to be computed in order to include the aforementioned defect-induced softening effects at the prototypical levels of defect concentrations. Application of this procedure yielded the lower-bound and upper-bound compressive transverse stress vs transverse stretch curves shown in Figure 16. Examination of the results shown in this figure reveals that the predicted range of the transverse compressive stresses at each transverse stretch level brackets the experimental value. However, the predicted lower-bound/upper-bound stress range is quite large, hampering full quantitative validation of the present computational procedure. Nevertheless, the present work clearly revealed the origin of the experimentally observed unusual concave-upward shape of the compressive transverse stress vs transverse stretch curve. That is, at small stretch values, the stress levels are dominated by the "softer" PPTA fibrils (i.e. the fibrils which are loaded in the edge-on mode) while, at large stretches, the same strength becomes increasingly controlled by the "hard" PPTA fibrils (i.e. the fibrils subjected to normal transverse compression).

4.2 Mechanical properties of PPTA fibers

In accordance with Figure 4(b), fibers are considered as assemblies of nearly parallel fibrils bonded, in the lateral direction, mainly via van der Waals forces. As established earlier, while PPTA sheets within all fibrils of a given fiber run parallel to the fiber axis, the orientation distribution of the sheet-normals, within a plane normal to the fiber axis, is typically assumed to be of a random nature. Consequently, it is generally assumed, as will be done in the present work, that the PPTA fibers behave as transversely isotropic materials (with the fiber axis being the

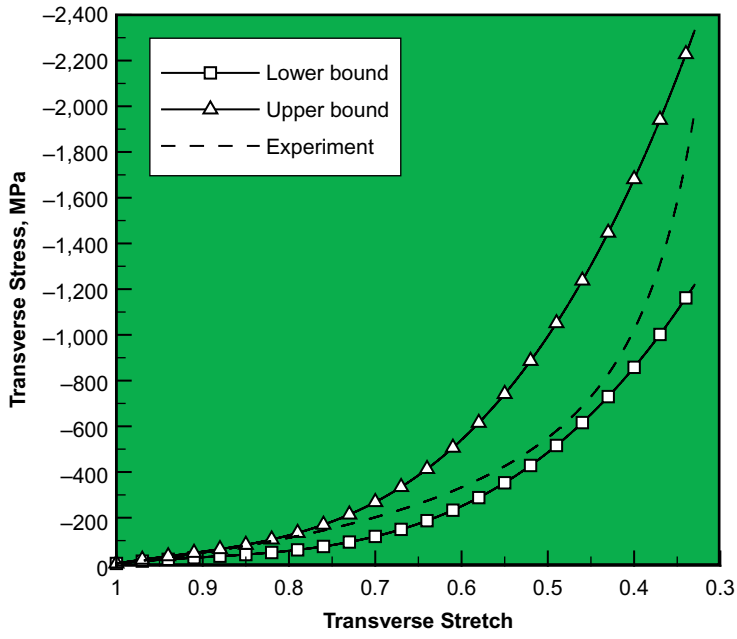

Figure 16.
Computed results pertaining to the lower-bound and upper-bound averaged compressive transverse stress vs transverse stretch data for PPTA effective fibrils

unique material direction). To derive the PPTA fiber-level material properties from the constituent PPTA fibril-level material properties, the following four-step procedure was applied:

(1) in the longitudinal direction, the fiber Young's modulus, E_{11}, and tensile strength, σ_1^T properties are set equal to their fibril counterparts;

(2) in the transverse direction, the Young's moduli, $E_{22} = E_{33}$, are determined by setting them equal to their fibril effective counterparts, as computed using the aforementioned Voigt and Reuss averaging procedures;

(3) the same Voigt and Reuss averaging procedures are used to compute G_{23} fiber shear modulus from its fibril counterpart; and

(4) the remaining two shear moduli G_{12} and G_{13} are set equal to the same value, which is controlled by the compliant PPTA inter-sheet sliding resistance (i.e. G_{12} of the fibrils).

The procedure utilized enables determination of the mechanical response of PPTA fibers under general loading conditions and, hence, plays a critical role in the construction of a yarn-level material model (discussed in the next section).

4.3 Mechanical properties of PPTA yarns

When structural/ballistic performance of fabric-based structures is analyzed computationally, it is a customary practice to model the fabric at a yarn-level resolution, i.e. the woven structure of the fabric is recognized by explicitly accounting for the presence of warp and weft yarns. In such computational analyses, yarns are assumed to be made of a continuum material. In other words, no account is taken of the effects of the underlying fiber-structure/topology and fiber contact/interactions. Derivation of the PPTA yarn continuum material models is beyond the scope of the present work. However, details regarding such a derivation including the phenomena such as fiber juxtaposition, yarn-twist-enhanced inter-fiber contact/friction, weak inter-fiber lateral bonding, etc. can be found in our prior work (Grujicic *et al.*, 2011b). The procedure presented by Grujicic *et al.* (2011b) showed that the yarn-level material properties are dependent on the fibril/fiber (crystallographic/morphological defects-controlled) properties as well as on the details of yarn architecture (e.g. the extent of yarn twist).

5. Summary and conclusions

Based on the results obtained in the present work, the following summary remarks and main conclusions can be drawn:

(1) Mechanical (specifically transverse elastic stiffness and compressive strength) properties of PPTA fibrils are investigated computationally using all-atom molecular statics and dynamics methods.

(2) In order to ensure that the computational model accurately represents the microstructure encountered in PPTA fibrils/fibers, consideration is given to the presence of various crystallographic/topological defects and their effect on the PPTA fibril/fiber mechanical properties.

(3) Due to the stochastic nature of the distribution of the defects' number density and potency, the PPTA strength properties are found to be also of a stochastic nature.

(4) Transverse elastic stiffness and compressive strength properties of PPTA fibrils are found to be greatly dependent on:
   - the orientation of the PPTA sheet-normal within the fibril; and
   - the type, local number density, clustering and potency of the defects.

(5) By accounting for the topological relationship between PPTA fibrils and fibers, fiber mechanical properties are derived using the appropriate averaging schemes. This procedure established that the computational analysis yields mechanical property data which are fairly consistent with the experimental counterparts.

References

Blades, H. (1973), US Patent 3,767,756.

Cheng, M. and Chen, W. (2006), "Modeling transverse behavior of Kevlar® KM2 single fibers with deformation-induced damage", *International Journal of Damage Mechanics*, Vol. 15, pp. 121-132.

Cheng, M., Chen, W. and Weerasooriya, T. (2004), "Experimental investigation of the transverse mechanical properties of a single Kevlar® KM2 fiber", *International Journal of Solids and Structures*, Vol. 41, pp. 6215-6232.

Cheng, M., Chen, W. and Weerasooriya, T. (2005), "Mechanical properties of Kevlar® KM2 single fiber", *Journal of Engineering Materials and Technology*, Vol. 127, pp. 197-203.

Cunniff, P.M. and Ting, J. (1999), "Development of a numerical model to characterize the ballistic behavior of fabrics", *Proceedings of the 18th International Symposium on Ballistics, San Antonio, TX*, pp. 814-821.

Dobb, M.G., Johnson, D.J. and Saville, B.P. (1977), "Supramolecular structure of a high-modulus polyaromatic fiber (Kevlar 49)", *Journal of Polymer Science: Polymer Physics Edition*, Vol. 15, pp. 2201-2211.

Dobb, M.G., Johnson, D.J. and Saville, B.P. (1981), "Compressional behavior of Kevlar fibers", *Polymer*, Vol. 22, pp. 960-965.

du Pont, E.I. (1983), "Weight savings for aircraft using Kevlar aramid fiber", Technical Brochure.

Edmunds, R. and Wadee, M.A. (2005), "On Kink banding in individual PPTA fibers", *Composites Science and Technology*, Vol. 65, pp. 1284-1298.

Grujicic, M. and Lai, S.G. (1999), "Kinetic Monte Carlo modeling of chemical vapor deposition of (111)-oriented diamond film", *Journal of Materials Science*, Vol. 34, pp. 7-20.

Grujicic, M., Cao, G. and Roy, W.N. (2004), "Atomistic modeling of solubilization of carbon nanotubes by non-covalent functionalization with poly (*p*-phenylenevinylene-Co-2, 5-dioctoxy-m-phenylenevinylene)", *Applied Surface Science*, Vol. 227, pp. 349-363.

Grujicic, M., Pandurangan, B., Koudela, K.L. and Cheeseman, B.A. (2006), "A computational analysis of the ballistic performance of light-weight hybrid-composite armors", *Applied Surface Science*, Vol. 253, pp. 730-745.

Grujicic, M., He, T., Marvi, H., Cheeseman, B.A. and Yen, C.-F. (2010a), "A comparative investigation of the use of laminate-level Meso-scale and fracture-mechanics enriched Meso-scale composite-material models in ballistic resistance analyses", *Journal of Materials Science*, Vol. 45, pp. 3136-3150.

Grujicic, M., Pandurangan, B., Snipes, J.S., Yen, C.-F. and Cheeseman, B.A. (2013), "Multi-length scale enriched continuum-level material model for Kevlar®-fiber reinforced polymer-matrix composites", *Journal of Materials Engineering and Performance*, Vol. 22, pp. 681-695.

Grujicic, M., Bell, W.C., Glomski, P.S., Pandurangan, B., Yen, C.-F. and Cheeseman, B.A. (2011a), "Filament-level modeling of aramid-based high performance structural materials", *Journal of Materials Engineering and Performance*, Vol. 20, pp. 1401-1413.

Grujicic, M., Bell, W.C., Glomski, P.S., Pandurangan, B., Yen, C.-F. and Cheeseman, B.A. (2011b), "Multi-length scale computational derivation of Kevlar® yarn-level material model", *Journal of Materials Science*, Vol. 46, pp. 4787-4802.

Grujicic, M., Arakere, G., Bell, W.C., Marvi, H., Yalavarthy, H.V., Pandurangan, B., Haque, I. and Fadel, G.M. (2010b), "Reliability-based design optimization for durability of ground-vehicle suspension-system components", *Journal of Materials Engineering and Performance*, Vol. 19, pp. 301-313.

Grujicic, M., Hariharan, A., Pandurangan, B., Yen, C.-F., Cheeseman, B.A., Wang, Y., Miao, Y. and Zheng, J.Q. (2012), "Fiber-level modeling of dynamic strength of Kevlar® KM2 ballistic fabric", *Journal of Materials Engineering and Performance*, Vol. 21, pp. 1107-1119.

Hearle, J.W.S., Lomas, B., Cooke, W.D. and Duerden, I.J. (1989), *Fibre Failure and Wear of Materials: An Atlas of Fracture Fatigue and Durability*, Wiley, Chichester.

Holzapfel, G.A., Stadler, M. and Ogden, R.W. (1999), "Aspects of stress softening in filled rubbers incorporating residual strains", in Dorfmann, A. and Muhr, A. (Eds), *Constitutive Models for Rubber*, A.A. Balkema, Rotterdam, pp. 189-193.

Johnson, G.R., Beissel, S.R. and Cunniff, P.M. (1999), "A computational model for fabrics subjected to ballistic impact", *18th International Symposium on Ballistics, San Antonio, TX*, CRC Press, Boca Raton, FL, pp. 962-969.

Johnson, G.R., Beissel, S.R. and Cunniff, P.M. (2002), "A computational approach for composite materials subjected to ballistic impact", *2nd International Conference on Structural Stability and Dynamics 2002*, World Scientific Publishing Company, Singapore, pp. 939-948.

Knoff, W.F. (1987), "A modified weakest-link model for describing strength variability of Kevlar aramid fibers", *Journal of Materials Science*, Vol. 22, pp. 1024-1030.

Konopasek, L. and Hearle, J.W.S. (1977), "The tensile fatigue behaviour of para-orientated aramid fibers and their fracture morphology", *Journal of Applied Polymer Science*, Vol. 21, pp. 2791-2815.

Kwolek, S.L. and du Pont, E.I. (1972), "Optically anisotropic aromatic polyamide dopes", US Patent No. 3,671,542.

Lim, C.T., Shim, V.P.W. and Ng, Y.H. (2003), "Finite-element modeling of the ballistic impact of fabric armor", *International Journal of Impact Engineering*, Vol. 28, pp. 13-31.

Lim, J., Zheng, J.Q., Masters, K. and Chen, W. (2011), "Effects of gage length, loading rates, and damage on the strength of PPTA fibers", *International Journal of Impact Engineering*, Vol. 38, pp. 219-227.

Materials Studio (2009), *Discover Theory Manual*, Accelrys Inc., Princeton, NJ.

Morgan, R.J., Pruneda, C.O. and Steele, W.J. (1983), "The relationship between the physical structure and the microscopic deformation and failure processes of poly (*p*-phenylene terephthalamide) fibers", *Journal of Polymer Science: Polymer Physics Edition*, Vol. 21, pp. 1757-1783.

Newell, J.A. and Sagendorf, M.T. (1999), "Experimental verification of the end-effect Weibull model as a predictor of the tensile strength of Kevlar 29 (poly *p*-phenylene terephthalamide) at different gage lengths", *High Performance Polymers*, Vol. 11, pp. 297-305.

Panar, M., Avakian, P., Blume, R.C., Gardner, K.H., Gierke, T.D. and Yang, H.H. (1983), "Morphology of poly (*p*-phenylene terephthalamide) fibers", *Journal of Polymer Science: Polymer Physics Edition*, Vol. 21, pp. 1955-1969.

Roylance, D. (1973), "Wave propagation in a viscoelastic fiber subjected to transverse impact", *ASME Journal of Applied Mechanics*, Vol. 40, pp. 143-148.

Shim, V.P.W., Lim, C.T. and Foo, K.J. (2001), "Dynamic mechanical properties of fabric armour", *International Journal of Impact Engineering*, Vol. 25, pp. 1-15.

Steenbakkers, L.W. and Wagner, H.D. (1988), "Elasticity and mechanical breakdown of Kevlar 149 aramid fibers by probabilistic approach", *Journal of Materials Science Letters*, Vol. 7, pp. 1209-1212.

Sun, H. (1998), "COMPASS: an *ab initio* force-field optimized for condensed-phase applications-overview with details on alkane and benzene compounds", *Journal of Physical Chemistry B*, Vol. 102, pp. 7338-7364.

Sun, H., Ren, P. and Fried, J.R. (1998), "The compass force field: parameterization and validation for phosphazenes", *Computational and Theoretical Polymer Science*, Vol. 8, pp. 229-246.

Taylor, W.J. Jr and Vinson, J.R. (1990), "Modeling ballistic impact into flexible materials", *AIAA Journal*, Vol. 28, pp. 2098-2103.

Wadee, M.A. and Edmunds, R. (2005), "Kink band propagation in layered structures", *Journal of the Mechanics and Physics of Solids*, Vol. 53, pp. 2017-2035.

Wadee, M.A., Hunt, G.W. and Peletier, M.A. (2004), "Kink band instability in layered structures", *Journal of the Mechanics and Physics of Solids*, Vol. 52, pp. 1071-1091.

Web sites

www.accelrys.com/mstudio/ms modeling/visualiser.html
www.accelrys.com/mstudio/ms modeling/amorphouscell.html

About the authors

Mica Grujicic is a Professor, Mechanical Engineering, Clemson University. Mica Grujicic's research interests include computational engineering. Mica Grujicic is the corresponding author and can be contacted at: gmica@clemson.edu

Subrahmanian Ramaswami is a Post-doctoral Fellow, Mechanical Engineering, Clemson University. Subrahmanian Ramaswami's research interests include computational material modeling.

Jennifer Snipes is a Post-doctoral Fellow, Mechanical Engineering, Clemson University. Jennifer Snipes' research interests include computational material modeling.

Ramin Yavari is a graduate student, Mechanical Engineering, Clemson University. Ramin Yavari's research interests include multi-physics modeling of various materials phenomena and processes.

Gary Lickfield is a Professor, Materials Science and Engineering, Clemson University. Gary Lickfield's research interests include online characterization during melt spinning.

Chian-Fong Yen is a Research Engineer, Army Research Labs, Aberdeen Proving Ground. Chian-Fong Yen's research interests include composite modeling.

Bryan Cheeseman is a Research Engineer, Research Labs, Aberdeen Proving Ground. Bryan Cheeseman's research interests include blast modeling and simulation.